Title
Role of Clustering in Determining Spatial Organization at the Immunological Synapse

Author
Hartman, Nina Caculitan

Publication Date
2010

Peer reviewed|Thesis/dissertation

Role of Clustering in Determining Spatial Organization at the Immunological Synapse

by

Niña Caculitan Hartman

A dissertation submitted in partial satisfaction of the

requirements for the degree of

Doctor of Philosophy

in

Chemistry

in the

Graduate Division

of the

University of California, Berkeley

Committee in charge:

Professor Jay T. Groves, Chair
Professor John Kuriyan
Professor Daniel A. Fletcher
Professor Jamie H.D. Cate

Spring 2010

Role of Clustering in Determining Spatial Organization at the Immunological Synapse

By

Niña Caculitan Hartman

The dissertation of Niña Caculitan Hartman, titled Role of Clustering in Determining Spatial Organization at the Immunological Synapse is approved:

Chair _____ Date_____

_____ Date_____

_____ Date_____

_____ Date_____

University of California, Berkeley

Abstract

Role of Clustering in Determining Spatial Organization at the Immunological Synapse

by

Niña Caculitan Hartman

Doctor of Philosophy in Chemistry

University of California, Berkeley

Professor Jay T. Groves, Chair

Micron-scale assemblies of molecules are thematic in biology, although their mechanism of formation and exact functional role are oftentimes unknown. The immunological synapse (IS)—the gateway event to the body's initiation of an immune response against infection—is a hallmark example. T cell detection of pathogenic invasion on an antigen-presenting cell leads to the arrangement of receptor-ligand pairs into well-defined concentric zones referred to as supramolecular activation clusters (SMACs). The main signaling molecule, the T cell receptor (TCR), binds its specific foreign peptide-presenting ligand, major histocompatibility complex (pMHC). These complexes form a central cluster in the central SMAC (cSMAC) at the center of the intermembrane junction. Immediately surrounding the cSMAC is the peripheral SMAC (pSMAC), populated by a ring of leukocyte function associated antigen-1 (LFA-1) bound to intercellular adhesion molecule-1 (ICAM-1). In this dissertation, we determine how the final IS pattern emerges from a uniform distribution of receptor-ligand pairs. It is known that the actin cytoskeleton drives the centripetal transport of these proteins, but it is unclear how actin sorts them into their final destinations. We postulate that the large-scale sorting of proteins into the different SMACs is a natural consequence of smaller scale protein sorting into microclusters, which may contain hundreds of molecules. To test this, we increase the LFA-1 cluster size two additional degrees beyond its native state with antibody crosslinkers. We either crosslink LFA-1 directly or indirectly with antibodies against its ICAM-1 ligand, which is presented on a supported membrane with the activating pMHC. Progressively more central localization of LFA-1 proportional to the degree of crosslinking results until LFA-1 occupies the cSMAC with TCR. Based on these results, we propose a sorting mechanism based on frictional protein coupling to actin. In the frictional force coupling model, the extent of radial protein transport by actin is determined by the specific coupling chemistry and the protein cluster size. This model predicts cluster size-based protein sorting across the IS. Using fluorescence fluctuation measurements and a small illumination area, we detect a gradient of LFA-1:ICAM-1 cluster sizes across the pSMAC in the native IS, as predicted by our model. Thus, we demonstrate that the well-regulated event of protein clustering is a critical parameter in regulating spatial patterning in the IS.

Contents

Acknowledgments

First and foremost, I would like to thank my advisor, Professor Jay Groves. His unique mentoring style, patience, and encouragement have allowed me to mature into an independent and relentless scientist. The Groves lab members—especially with their own quirks and eccentric ways of thinking—have been a delight to work and commiserate with, especially during the most stressful times of my graduate life. I don't think I'll ever encounter a group of people who are as sharp and as caring in my scientific career. The lab serves as a living example that the sum is greater than its parts, and I hope that this culture continues long after I leave.

I would like to specifically acknowledge the people involved in my projects, Jeff Nye, Cheng-han Yu, Wan-Chen Lin, Theo Lohmueller, Joe Hickey, Eulanca Liu, and Nicole Fay. You have taught me so much about science, life, and Germany. Also, special thanks to Pradeep Nair, whose kindness and eternal patience has helped maintain the balance of forces in the lab.

Finally, I am deeply grateful for those who have made my life more livable. Wan-Chen and Selva, thank you for welcoming me into your home when I simply did not have the energy or time to make my long commute. I am honored to have witnessed your relationship blossom and flourish. Luke, I will forever cherish our many food breaks when we chatted about nothing and everything. To my family, thank you for your constant support. And Jared, you keep my mind open to different ways of seeing the world and are a constant reminder of the importance of balancing work and play.

Chapter 1

Introduction

1.1 Abstract

This chapter briefly describes the discovery and development of the immunological synapse (IS)—an intercellular junction formed between T cells and antigen presenting cells. It specifically highlights the use of model membranes to investigate spatial transport and signaling events in the nascent and mature IS. The bottom up approach to ligand presentation and simplified imaging interface conferred by the supported membrane system is amenable to quantitative studies of T cell triggering. In addition, the many lithographic techniques that make it possible to manipulate spatial organization within the IS makes it an ideal platform for investigating the mechanism behind IS formation. Current knowledge and research directions in the study of the IS are also discussed.

1.2 T Cells and Adaptive Immunity

T cells are the first line of defense in the adaptive immunity—a well-orchestrated series of events that eliminates large-scale infection and prevents recurrences in the future. Many types of T cells exist and clones of each type respond only to a specific pathogenic signature. The role T cells is to scavenge the body and look for signs of pathogenic invasion. Infection is presented as digested peptides on the surface of antigen presenting cells (APCs). The peptides may be derived from endocytosed antigen or antigen that has invaded the APC and hijacked the protein machinery. Upon activation, helper T cells proliferate and recruit other cells to mediate the clearance of the infection, whereas cytotoxic T cells kill infected cells on contact. In spite of the different cell fates, both have a similar method of recognition; T cell receptors (TCR) bind their cognate ligands, major histocompatibility complexes (MHC), and the antigen-derived peptides they present (Fig. 1). During organismic development, the body may produce up to 10^6 types of T cells all with T cell receptors that are sensitive to only one kind of foreign antigen and none of which should react to self-derived peptides [1]. The whole process of producing and selecting T cell clones with such specificity and sensitivity is a well-studied area of research. However, this work will focus more on how the detection of the activating pMHC complex is transformed to helper T cell triggering.

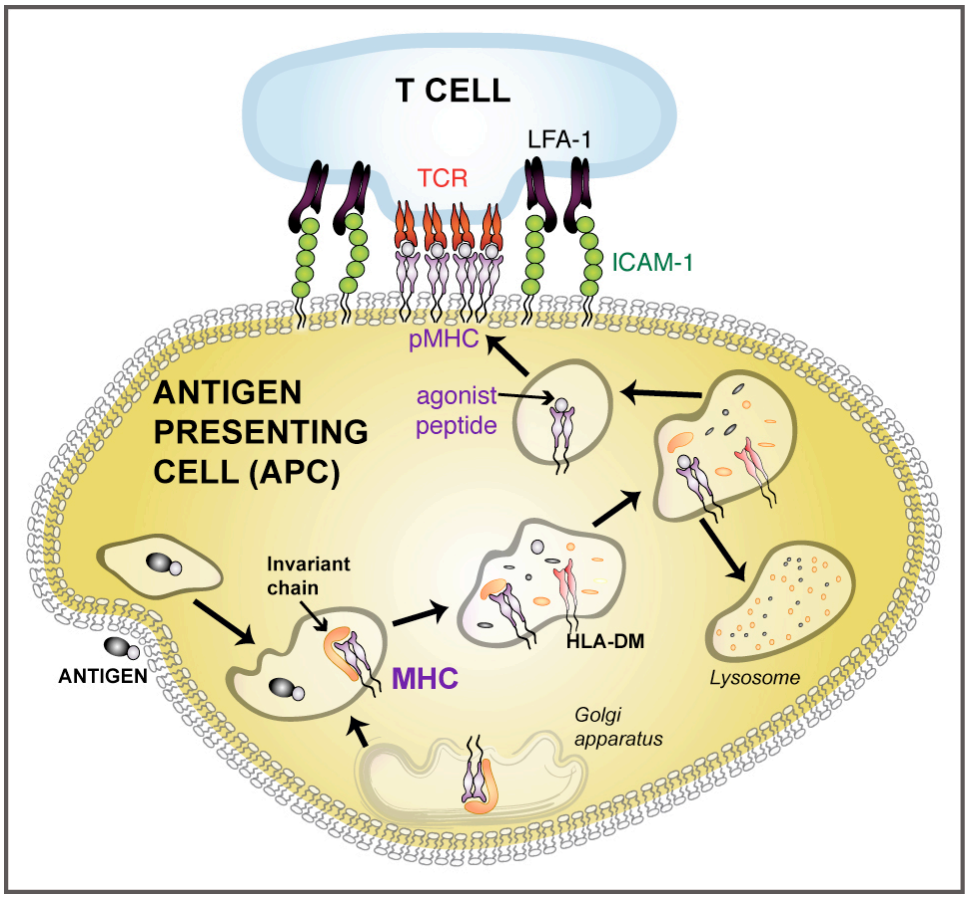

Figure 1.1: Antigen presentation by the APC and helper T cell detection. The antigen is endocytosed by the APC and digested in vesicles to be loaded on the MHC protein. Premature loading of the antigen is prevented by the presence of the invariant chain. The presence of the HLA-DM protein helps to catalyze peptide loading onto the MHC. The pMHC complex is then shuttled to the cell membrane by vesicular transport.

1.3 The Immunological Synapse

The methods used to study T cell activation have evolved hand in hand with the development of various biochemical and biophysical techniques. More than 30 years ago, immunologists began to investigate "cell-mediated" immunity, wherein cytotoxic T cells can induce lysis of foreign or infected cells [2]. Much effort was focused on investigating the many receptors involved via different biochemical assays, and a favorite among biologists was the newly developed antibody-binding assay [3]. The ability to produce virtually pure solutions of monoclonal T cell clones gave way to the production of antibody libraries against molecules on the T cell surface. In the early 1980s, several investigators coupled this technique with co-immunoprecipitation assays and identified the TCR αβ chains as the primary receptor responsible for antigen recognition [4,5]. Around the same time, Springer et al. also discovered that blocking the binding of the adhesion molecule lymphocyte function associated antigen-1 (LFA-1) with an antibody severely impaired T cell function [6]. Other important associated and costimulatory molecules, such as CD8, CD4, and CD2, were also discovered in a similar manner [7]. By the late 1990s, full or partial crystal structures of some these molecules made possible the study of the molecular details of the purified proteins, sometimes with their respective ligands [8,9,10,11,12]. Scientists had hoped that knowing the intricacies of the intermolecular interactions would unlock the mysteries behind T cell triggering. However, knowledge of the molecular scale phenomena did not readily explain exactly how all the molecules

involved acted synergistically to initiate the immune response.

In the late 1990s, fluorescent labeling of proteins and visualization of the T cell-APC intercellular junction with confocal microscopy led to the discovery of the "immunological synapse" (IS) [13]. First identified by Kupfer et al., the IS is the large-scale sorting of membrane proteins bound to their respective ligands into well defined and segregated concentric domains. These domains were thought to be crucial to T cell activation and were therefore aptly called supramolecular activation clusters (SMACs). The TCR:pMHC complexes form a central cluster within the central SMAC (cSMAC) surrounded by a ring of LFA-1 bound to its ligand, intercellular adhesion molecule-1 (ICAM-1) within the peripheral SMAC (pSMAC). Beyond the pSMAC is the distal SMAC (dSMAC), which is occupied by large glycoproteins such as CD44, CD45, and CD46 [14,15]. Various adaptor proteins and signaling molecules may also be found associated with the membrane proteins at the different SMACs (Fig. 1.2A) [15]. This visually striking protein pattern forms within minutes of TCR recognition of agonist peptide presentation by the MHC ligand on the APC. (Fig. 1.2B). It is known that the lack of IS formation results in little to no T cell response. Subsequent studies revealed that the same proteins formed different patterns at other immune cell interfaces [16,17,18,19]. For example, immature T cells or thymocytes form a multifocal pattern of TCR:pMHC microclusters in a sea of LFA-1:ICAM-1 complexes [19]. On the other hand, natural killer cells appear to form inverted synapses [17]. These different spatial patterns may also lead to distinct outcomes, such as negative selection and lysis of target cell. Thus, micron-scale assemblies of proteins at immune synapses may be the determinants of T cell activation, proper modulation of downstream signaling, and ultimate cellular output. Although much is known in terms of the key players, the dynamics, and spatial aspects of the IS, two key questions remain unanswered: how and why does the IS form?

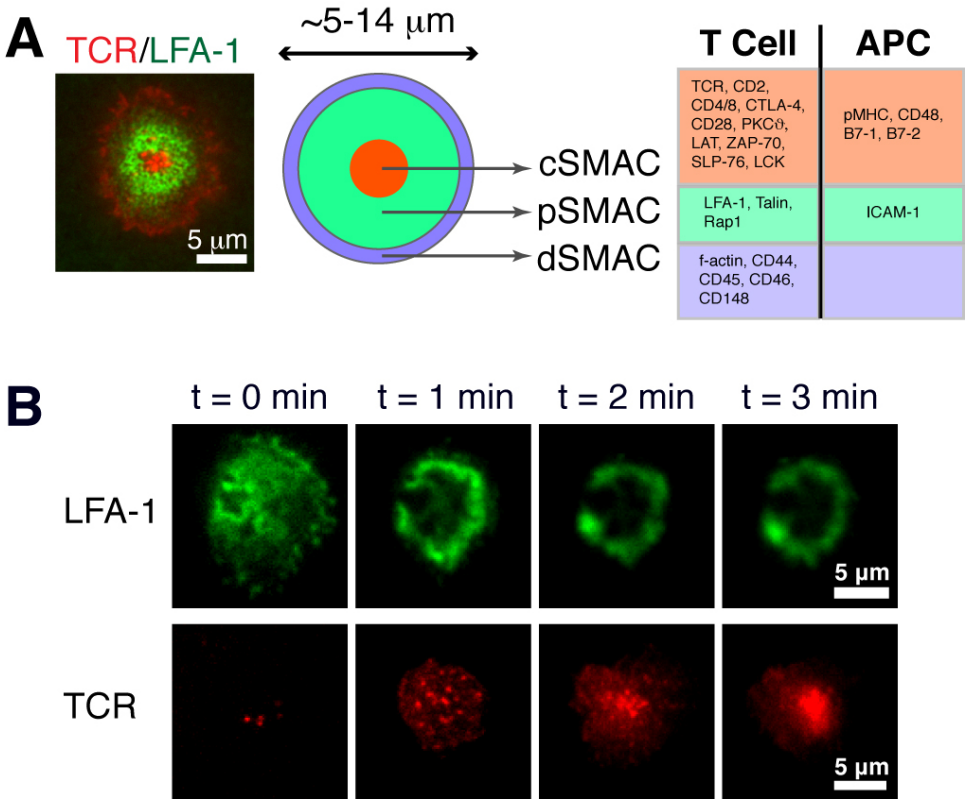

Figure 1.2: Protein spatial patterning during IS formation. **(A) Left**, Differential sorting in the IS of fluorescently labeled TCR (red) and LFA-1 (green). **Center**, Schematic of the different zones within a typical cell. **Right**, List of the various proteins that are sorted into the different SMACs. **(B)** Time-lapse images of IS formation imaged with fluorescently labeled LFA-1 (green) and TCR (red).

1.4 Studying the IS with Model Membranes

The year following Kupfer's discovery of the IS, Dustin et al. recapitulated the system in a hybrid live T cell-supported lipid bilayer (SLB) experimental platform [20]. Here, the APC is replaced by a fluid membrane deposited on a glass substrate and displaying GPI-linked pMHC and ICAM-1. Findings by Wulfing et al. demonstrated that only the actin cytoskeleton of the T cell was necessary for IS formation, giving way to this simplification [21]. Although Dustin et al. were the first image the IS with this platform, model membranes have been used to study T cell activation of several decades preceding this work [22,23]. However, several experimental limitations needed to be overcome, the most important of which was lack of lateral fluidity. Previous experiments had incorporated transmembrane proteins into the bilayer, which led to non-fluid protein islands [24,25,26]. While these studies were effective in observing T cell function, other experiments suggest that lateral fluidity is necessary for full T cell activation [27,28]. Fluid presentation of proteins was achieved by incorporation of glycosylphosphatidylinositol (GPI)-linked proteins, which interact only with the top leaflet of the bilayer [29]. Since then, different protein tethering techniques have been developed. These include streptavidin coupling of biotinylated proteins and lipids[30,31], Ni^{2+} chelating lipids anchoring histidine-tagged proteins[32,33], DNA hybridization[34,35] and many others.

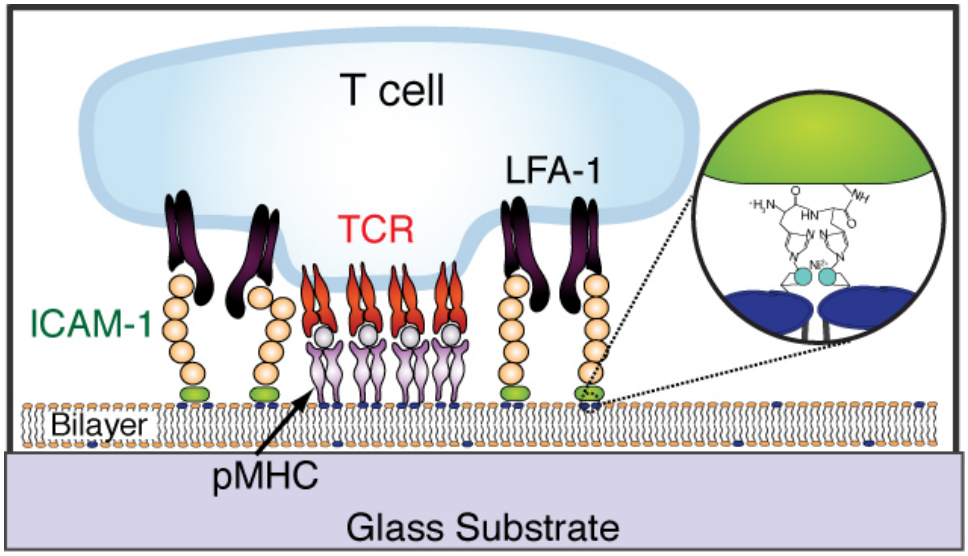

Figure 1.3: The APC is replaced by a fluid supported lipid bilayer presenting pMHC and ICAM-1 ligands to the T cell. Here, Ni^{2+} chelating lipids anchor oligohistidine-tagged proteins to the SLB.

The SLB offers several advantages that make it amenable for dissecting the specific role of large-scale protein sorting on cell signaling. First, the well-defined imaging plane allows the use of advanced microscopy to specifically probe the intermembrane junction with little background. Second, the fluid nature of the bilayer and tunable control over ligand presentation facilitates the quantitative investigation of costimulatory molecules' effect on T cell activation. Third, real-time tracking of IS dynamics is made possible. Finally, manipulations, which we refer to as spatial mutations, can be directly applied to the substrate to dissect the native spatial protein patterning without perturbing other interactions in the cell. One example is the presentation of diffusion barriers in the form of chromium lines deposited by electron beam lithography to prevent movement of lipids and ligands across the barriers [36]. In turn, bound cognate receptors are laterally restricted. The planar surface of the substrate may also be modified to present nanometer-scale curvature that may redirect protein translocation [37]. Artificial segregation or congregation of ligands may be induced by immobilization on the substrate [38], or via the creation of micron-scale, ligand-specific areas within the SLB [39] (Fig. 1.3).

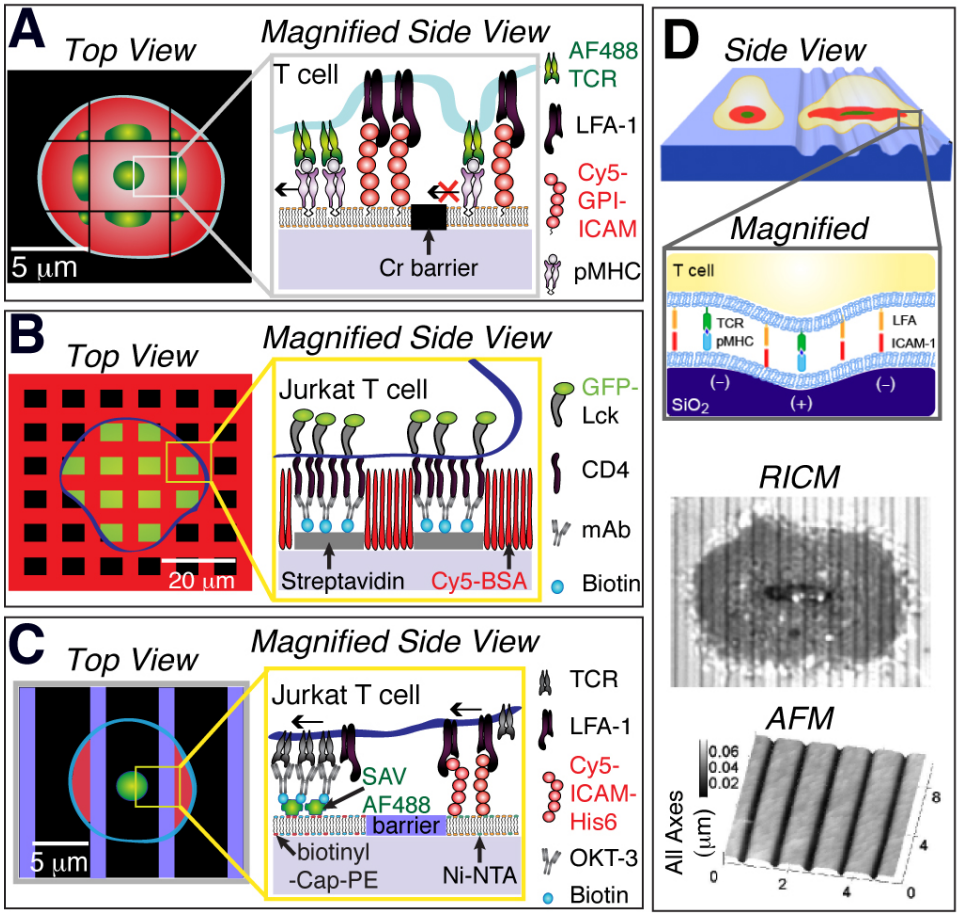

Figure 1.4: Examples of different spatial mutations that may be applied to the hybrid live T cell-SLB system. **(A) Left,** LFA-1:ICAM-1 (red) and TCR:pMHC (green) complexes on 5 μm grids. **Right,** Chromium lines act as diffusion barriers, restricting lateral movement of receptor-ligand pairs that encounter them. **(B) Left,** Photolithography is used to immobilize proteins in specific patterns on a background of a passivating protein, such as BSA (red). **Right**, Jurkat T cell expressing intracellular Lck-GFP selectively interacts with immobilized CD4 on the underlying substrate. **(C) Left,** Microfluidic channels are used to create interdigitated bilayers several microns in width and presenting different ligands. **Right**, Receptors on the Jurkat T cell selectively interact with their ligands presented on each bilayer. **(D) Top images,** Areas of the glass substrates undergo anisotropic etching to produce nanometer-scale curvatures. The T cell membrane follows the curvature. **Bottom images**, reflection interference contrast microscopy (RICM) image of cell forming an IS on curved substrates. Scanned atomic force microscopy (AFM) image of curved substrate. These images reveal the topography of the curved substrates. Adapted from reference 39.

1.5 Current Knowledge about the IS

Many speculated that the TCR cSMAC acted as a signal amplification center for cell signaling. However, Lee et al. have shown that TCR signaling occurs before TCR:pMHC microclusters congregate at the cSMAC[40]. In the groundbreaking work of Mossman et al., the use of metal lines as diffusion barriers (Fig. 1.4A) proved that TCR signaling in microclusters was actually prolonged when confined to the periphery and attenuated upon reaching the cSMAC [36]. However, the signaling motif may be determined by activation strength. Shaw et al. found that the cSMAC can become the site of sustained phosphorylation in the presence of low agonist concentration [41]. The spatial dependence of early versus late stage phosphorylation has also been detected [42]. Thus, it appears that protein spatial organization can regulate initial cell signaling.

Spatial mutations have also been useful in determining the minimum number of agonist peptide-MHC molecules needed for T cell triggering. Manz et al. use increasingly small grids of diffusion barriers down to 0.25 um^2 to titrate down the number of agonist peptide-MHC presented to the T cell [43]. In this work, four agonist-pMHC molecules is the minimum number to induce Ca^{2+} flux, a digital indicator of cell activation (Manz). One of the challenges faced in this work was less than ideal bilayer fluidity and artificial clustering due to unfused vesicles of GPI-linked proteins. The change from GPI-anchored to Ni^{2+}-histidine coupling of proteins to the bilayer produced a superior bilayer without these problems.

Current research now focuses on determining the molecular content of the minimum TCR microcluster unit and how clusters of signaling molecules, such as LAT, lck, SLP-76, etc. become associated with it [44,45,46,47,48]. Furthermore, in protein patterning experiments, antibodies against costimulatory molecules on the T cell are immobilized along with pMHC to determine how the final protein pattern can affect cell signaling [49]. These experiments yield interesting results in terms of the effect of protein location and segregation on cell signaling. However, the current methodologies used do not allow for micro-scale receptor lateral mobility or sometimes present cells with antibodies in solution, which can induce clustering on their own. Past research underscores the importance of spatial location and microcluster formation to cell signaling. Therefore, it is clear that improvements addressing these limitations are necessary to truly understand the implications of the IS in cell signaling and adaptive immune responses.

1.6 The Role of the Actin Cytoskeleton in the IS

The actin cytoskeleton has long been suspected to play a role in the spatial rearrangement of proteins into the canonical bull's eye pattern of the IS. Traditionally, studies have focused on the effects of pharmacological inhibitors, which disrupt actin polymerization, on IS formation [21]. Results strongly show that actin is important not only in transporting TCR:pMHC complexes but also in the nucleation of TCR-pMHC microclusters[50]. Interestingly, not all receptor-ligand pairs at the IS are clustered in the same manner or to the same degree. For example, LFA-1 does not appear to form clusters on the same scale as the TCR-pMHC microclusters when binding its ligand, ICAM-1. Single particle tracking of TCR microclusters on an open maze of diffusion barriers also provides insight into how clusters are coupled to actin. Instead of stopping abruptly upon encountering diffusion barriers, the speeds of TCR microclusters simply decrease in speed and easily change trajectories to find an opening. These findings suggest that TCR microclusters are only transiently, instead of permanently, coupled to actin [51]. By dynamically tracking fluorescently labeled proteins, Kaizuka et al.'s work supports the idea that both TCR microclusters and LFA-1:ICAM-1 complexes are "frictionally" coupled to the centripetal actin flow [30]. In their work, immortalized human T cells, commonly known as Jurkat cells, are exposed to a bilayer displaying anti-CD3 antibodies (instead of pMHC) and ICAM-1. Furthermore, they propose that differences in the cluster stabilities of TCR clusters versus LFA-1:ICAM-1 complexes lead to protein sorting. Specifically, actin deficiency in the cSMAC and the diffusion barrier imposed by the TCR-pMHC central cluster precludes the

entry of LFA-1:ICAM-1 complexes, confining them to the pSMAC. This is supported by the maintenance of the TCR-pMHC central cluster in spite of actin drugging with Latrunculin A, which resulted in the dissolution of the LFA-1:ICAM-1 ring in the pSMAC [30]. Another model proposes that the differences in molecular ectodomain sizes drive protein sorting [15]. Still, the exact mechanism of how actin flow is related to receptor transport in the IS remains a mystery.

1.7 Current Objectives

In this dissertation, I investigate the effect of protein cluster size on differential radial sorting. Although TCR and LFA-1 differ in their coupling chemistry to actin, it is possible that the disparity in their clustering propensities may be the key to their segregation into the cSMAC and the pSMAC, respectively. In the work presented, the cluster sizes of the LFA-1:ICAM-1 complexes are increased with antibody crosslinking. I elucidate how these differential cluster sizes regulate protein translocation in the IS and propose a frictional force coupling model to explain my results. In addition, I apply fluorescence fluctuation analysis on LFA-1 bound, fluorescent ICAM-1 molecules and determine the native distribution of LFA-1:ICAM-1 cluster sizes across the IS. My findings support the frictional force coupling model, which may be generalized to other proteins within the IS.

Chapter 2

Cluster Size Regulates Protein Sorting in the Immunological Synapse

Reproduced with permission from *Proceedings of the National Academy of Sciences USA* 106(31):12729-12734: "Cluster Size Regulates Protein Sorting in the Immunological Synapse", N. C. Hartman, J. A. Nye and J. T. Groves.

2.1 Abstract

During antigen recognition by T cells, signaling molecules on the T cell engage ligands on the antigen-presenting cell and organize into spatially distinctive patterns. These are collectively known as the immunological synapse (IS). Causal relationships between large-scale spatial organization and signal transduction have previously been established. Although it is known that receptor transport during IS formation is driven by actin polymerization, the mechanisms by which different proteins become spatially sorted remain unclear. These sorting processes contribute a facet of signal regulation; thus their elucidation is important for ultimately understanding signal transduction through the T cell receptor. Here we investigate protein cluster size as a sorting mechanism using the hybrid live T cell–supported membrane system. The clustering state of the costimulatory molecule LFA-1 is modulated, either by direct antibody crosslinking or by crosslinking its ICAM-1 ligand on the supported bilayer. In a mature IS, native LFA-1 generally localizes into a peripheral ring surrounding a central TCR cluster. Higher degrees of LFA-1 clustering, induced by either method, result in progressively more central localization with the most clustered species fully relocated to the central zone. These results demonstrate that cluster size directly influences protein spatial positioning in the T cell IS. We discuss a sorting mechanism, based on frictional coupling to the actin cytoskeleton, which is consistent with these observations and is, in principle, extendable to all cell surface proteins in the synapse.

2.2 Introduction

Despite their dynamic liquid nature, cell membranes exhibit distinctive spatial organization on length-scales ranging from molecular dimensions to the size of the cell itself. One particularly dramatic example is the T cell immunological synapse (IS). This structure is a specialized junction between a T cell and an antigen-presenting cell (APC), within which a variety of receptor and adhesion proteins engage their cognate ligands on the apposed cell surface [13,20]. Prior to contact, no large-scale organization is present on either cell surface. However, within minutes of the initial encounter between an APC displaying appropriate antigen and a complementary T cell, a highly coordinated transport process is initiated that ultimately sorts dozens of membrane proteins on both cell surfaces into a series of concentric rings. This spatial pattern of proteins is not unique to T cells; similar structures have also been observed between natural killer (NK) cells and B cells and their target cells as well as between certain immune cells and neurons [16-18]. Recent work has demonstrated the importance of protein spatial distribution to both effector functions and as a signal regulatory mechanism [36,40,52]. However, the mechanism of IS formation is unclear.

In the case of the T cell-B cell interaction, the rapid spatial sorting of cell membrane proteins into multiple specific regions within the intercellular junction is driven from within the T cell [21]. Substitution of the B cell with a synthetic supported lipid bilayer (SLB) displaying key proteins produces minimal differences in the antigen specificity or protein spatial organization [20]. The transport mechanism is postulated to be based on actin polymerization and the resulting centripetal actin flow within the T cell [30,50,53]. Disruption of this actin flow using cytoskeletal inhibitors blocks transport [30,53]. Associations of cell-surface proteins with actin are thought to exist via adaptor proteins, such as talin, which is known to couple lymphocyte function-associated antigen-1 (LFA-1) to the actin cytoskeleton [54]. Similarly, ezrin has been reported to be an adaptor protein for the T cell receptor (TCR) [55]. While simply coupling to actin flow may be sufficient for protein transport, additional regulation is required to achieve differential sorting of multiple proteins within the IS.

Differential protein sorting is markedly illustrated by comparison of TCR and LFA-1, which become segregated into the central supramolecular activation cluster (cSMAC) and the surrounding peripheral supramolecular activation cluster (pSMAC), respectively [13,20]. Direct tracking of TCR

and LFA-1 motion on the cell surface reveals that these two proteins move in the same direction under the influence of centripetal F-actin flow [30,51,53]. The mechanism directing them to different destinations, microns apart, remains mysterious. Prior to transport, TCR engagement of the peptide-major histocompatibility complex (pMHC) on the apposed membrane leads to the formation of TCR clusters, containing on the order of 100 TCR molecules, which are subsequently transported to the cSMAC [50,56]. LFA-1 does not form such large-scale clusters upon binding its ligand, intercellular adhesion molecule-1 (ICAM-1) [54,57]. Thus, we speculate that differences in cluster size may contribute to protein sorting.

In the following, we manipulate the clustered state of LFA-1 in primary murine T cells in order to directly investigate the effect of protein cluster size on spatial sorting. Cluster size is increased by crosslinking LFA-1 with a non-blocking bivalent monoclonal antibody (Bi-X LFA-1). Crosslinking the primary antibody with a secondary antibody to form a tetravalent crosslinker against LFA-1 leads to a more clustered state (Tetra-X LFA-1). Thus two degrees of clustering beyond the native state, which may already be clustered to a small degree, are accessible. Compared to non-crosslinked LFA-1, Bi-X LFA-1 is transported further inward toward the inner zone of the pSMAC, immediately surrounding the cSMAC. Crosslinking with a tetravalent agent leads to localization of LFA-1 to the cSMAC along with TCR. Use of bivalent and tetravalent crosslinkers against ICAM-1 induces similar alterations in the spatial position of LFA-1:ICAM-1 complexes. Thus, increasing the clustering state of LFA-1, either directly using anti-LFA-1 antibodies or indirectly by crosslinking its ICAM-1 ligand, biases its distribution toward the synapse center. Moreover, spatial sorting of the differentially cross-linked LFA-1 species from each other within a single synapse is also observed. These results illustrate that differences in protein cluster size are sufficient to direct discrete sorting of proteins into different regions of the IS. We discuss how a frictional mechanism for coupling of proteins to centripetal actin flow, which may apply generally to many proteins in the synapse, predicts this.

2.3 Results

2.3.1 ICAM-1 distribution reflects ligated LFA-1 pattern on the T cell

The formation of LFA-1:ICAM-1 complexes is necessary for the recruitment of active LFA-1 and ligated ICAM-1 to the pSMAC [52]. During cell migration and upon TCR activation, LFA-1 binds ICAM-1 and induces its accumulation on the apposed surface in contact with the T cell membrane [54]. This interaction depletes the local concentration of unbound ICAM-1 molecules, which further drives the diffusive flux of free ICAM-1 into the contact area by the law of mass action [58]. The total ICAM-1 distribution thus reflects the pattern of active, ligated LFA-1 on the T cell surface. To confirm that the ICAM-1 pattern provides a real-time means of tracking ligated LFA-1 on the T cell, we monitor its reversibility of binding to crawling T cells. We use an ICAM-1-YFP fusion protein linked to nickel-chelating lipids in the SLB by a stable decahistidine tag [33]. While the commonly used H155 antibody for LFA-1 also allows for direct tracking, it does not distinguish among all the different conformations of LFA-1 that may exist on the membrane. Thus, it indiscriminately binds both active (ICAM-1 bound) and inactive (non-ICAM-1 bound) forms of LFA-1 [59]. To quantitatively characterize ICAM-1 fluorescence as a function of its interactions with LFA-1 on T cells, we deposit the SLB on substrates pre-patterned with grid arrays of metal lines (3 μm x 3 μm corrals) that act as barriers to lateral mobility. Membrane lipids and proteins diffuse normally within each corral [36,60]. A constant number of freely mobile ICAM-1 molecules are thus trapped within each corral (Figs. 2.1 and 2.2) [61,62,63]. Restriction of ICAM-1 and pMHC lateral motion within the SLB by the metal grid lines indirectly disrupts the transport of bound cognate receptors on the T cell (Fig. 2.1A). Receptor-ligand pairs do not directly interact with the metal lines and are affected solely by restriction of their lateral mobility [36,60].

Initially, ICAM-1 accumulates beneath the crawling T cell and the area of ICAM-1 accumulation decreases in size as the cell migrates away from the corral. Without T cell contact (t=110 seconds, Figs. 2.1C and 2.2 A and B), ICAM-1 rapidly returns to a homogeneous distribution by passive diffusion. The total integrated fluorescence, relative to off grid ICAM-1, remains constant, confirming that fluorescence intensity linearly maps ICAM-1 concentration. The low variance in the integrated fluorescence intensities hold true for the ensemble data of cells interacting with many corrals (Figs. 2.2E and F). This indicates that no measurable quenching is observed nor does ICAM-1 desorb from the membrane over the course of these experiments. These results confirm that ICAM-1 spatial distribution quantitatively reflects the distribution of LFA-1:ICAM-1 complexes.

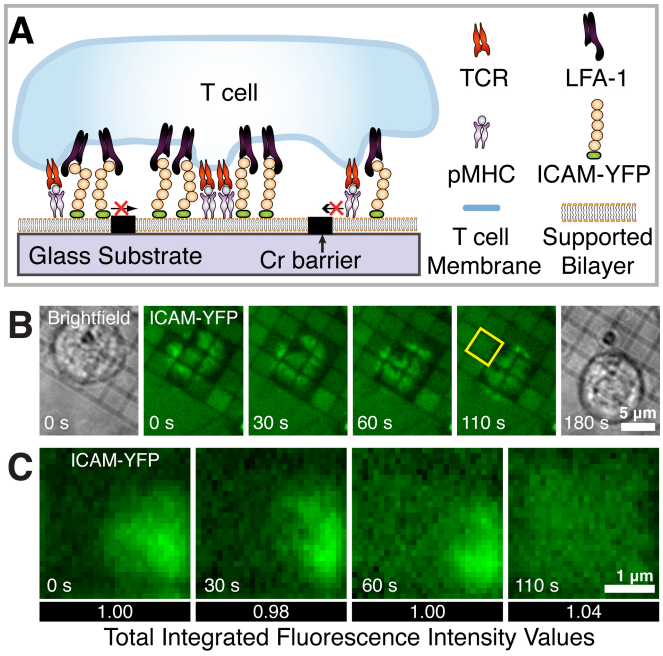

Figure 2.1: ICAM-1 distribution reflects the ligated LFA-1 pattern on the T cell. **(A)** Diagram of a T cell exposed to a planar bilayer on a patterned substrate. Proteins on the T cell engage their cognate ligands and are constrained by the diffusion barriers. **(B)** A cell migrates over a supported bilayer containing ICAM-1 and pMHC corralled by metal lines into 3 mm squares. As the cell moves, ICAM-1 distribution within the corrals changes as a result of LFA-1 binding. When the cell is no longer in contact with the grid square, ICAM-1 is released and diffuses back to homogeneity. **(C)** Magnified images of the 3 mm x 3 mm square indicated in (B). Total integrated fluorescence within the corral indicated, normalized to t = 0, is given beneath each image, showing that clustering does not significantly affect total ICAM-1 fluorescence.

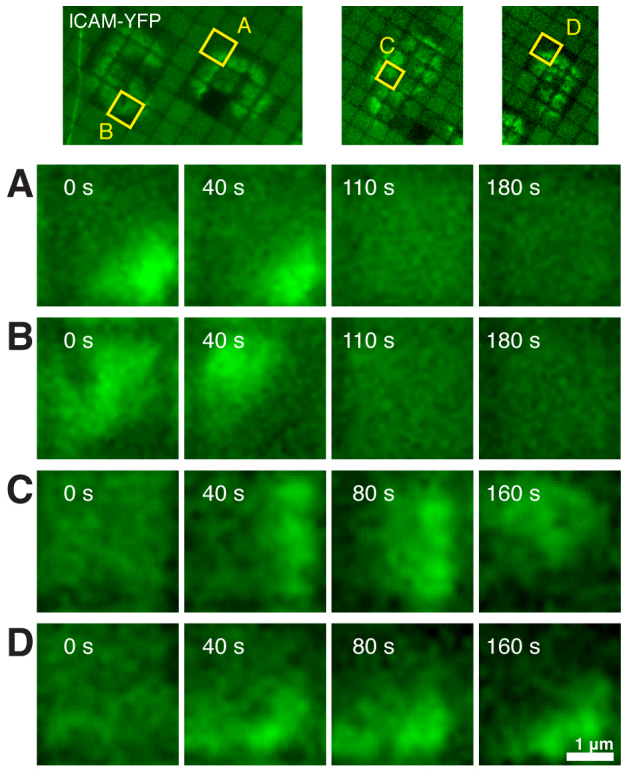

E

Region	Integrated Fluorescence				Ave±SE
A	1.000	1.000	1.003	1.003	1.002±0.001
B	1.000	0.999	1.000	1.004	1.000±0.002
C	1.000	0.999	1.003	1.005	1.002±0.003
D	1.000	1.003	1.002	1.002	1.003±0.001

F

Corral	Integrated Fluorescence				Ave±SE
1	1.000	1.014	1.012	1.007	1.010±0.001
2	1.000	1.015	1.016	1.011	1.013±0.001
3	1.000	1.015	1.017	1.010	1.013±0.001
4	1.000	1.012	1.014	1.007	1.010±0.001
5	1.000	1.012	1.012	1.007	1.010±0.001
6	1.000	1.017	1.014	1.008	1.012±0.001
7	1.000	1.012	1.012	1.008	1.010±0.001
8	1.000	1.012	1.012	1.009	1.010±0.001
9	1.000	1.014	1.014	1.009	1.011±0.001
10	1.000	1.002	1.005	0.990	1.001±0.001
11	1.000	0.994	0.989	0.984	0.992±0.002
12	1.000	0.999	0.992	0.985	0.994±0.002
13	1.000	1.006	1.013	1.019	1.010±0.002
14	1.000	1.001	0.998	0.991	0.997±0.001
15	1.000	1.002	1.002	1.002	1.003±0.001
16	1.000	1.004	1.009	1.010	1.007±0.001
17	1.000	1.000	0.996	0.992	0.998±0.001
18	1.000	1.006	1.010	1.010	1.008±0.001
19	1.000	1.000	0.995	0.987	0.997±0.001
20	1.000	1.006	1.016	1.016	1.010±0.001

Figure 2.2: Ensemble of four identically prepared cells migrating over bilayers containing ICAM-1 constrained by diffusion barriers. **(A-D)** Magnified images of the 3 mm x 3 mm square indicated in the cell images for four different cells. T cells migrate either onto (A,B) or off of (C,D) the corral. **(E)** Calculated values for the integrated fluorescence intensity (±SE) as a function of time for the region indicated. Final column shows the mean integrated fluorescence intensity values for each corral over the entire time series (20 frames, 2 min) normalized to t = 0. **(F)** Integrated intensities (±SE) for a sampling of corrals interacting with crawling cells as a function of time. Last column shows the mean values over the entire time series obtained as in E. All of the corrals with which other cells interact show similarly low variance in integrated fluorescence intensity, indicating that clustering does not significantly affect total ICAM-1 fluorescence.

2.3.2 LFA-1 is transported inward during IS formation

In the native IS, LFA-1:ICAM-1 complexes form a ring at the pSMAC and TCR:pMHC microclusters congregate into a central cluster at the cSMAC (Fig. 2.3A). Synapse assembly on substrates displaying diffusion barriers leads to altered protein patterns in the final IS, which we refer to as spatial mutations [36]. Specific features of the spatial mutation reveal aspects of the mechanism that drives synapse assembly. Here, the inward radial transport of both TCR:pMHC and LFA-1:ICAM-1 complexes is made apparent by TCR and ICAM-1 accumulation in areas along the grid lines that are closest to the synaptic center (Fig. 2.3B). Similar evidence of LFA-1 inward transport is observed by directly labeling LFA-1 with H155 antibody (Fig. 2.4). The time lapsed images indicate that LFA-1 adopts a ring pattern within a minute of T cell exposure to the bilayer. These observations confirm that both LFA-1 and TCR are transported in an inward radial manner during synapse formation in primary T cells by processes that resemble those previously reported from tracking experiments in Jurkat cells [30]. Disruption of the ring pattern by addition of the actin polymerization blocker, Latrunculin A, confirms that inward transport is mediated by actin centripetal flow (Fig. 2.5).

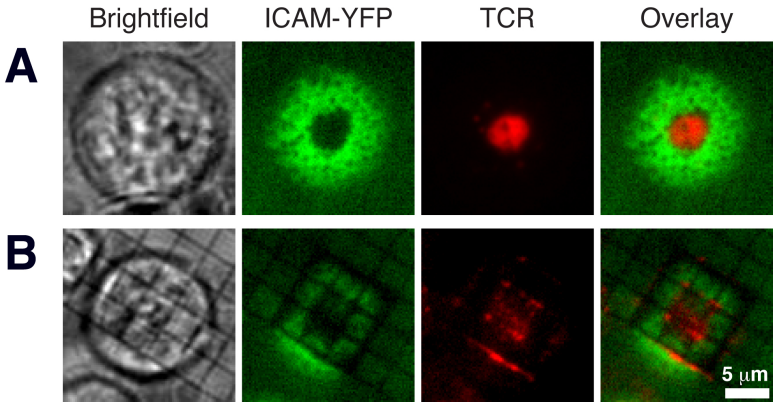

Figure 2.3: LFA-1 is transported inward during IS formation. **(A)** In an unperturbed IS, LFA-1:ICAM-1 complexes form a ring, as visualized with ICAM-YFP, and TCR labeled with H57 aTCR-f_{ab} (Alexa-Fluor 488) forms a central cluster (observed in 75% of T cells, n=81). **(B)** Upon T cell interaction with an SLB constrained by metal grid lines, LFA-1:ICAM-1 complexes and TCR accumulate in areas closest to the synaptic center (observed in 80% of T cells, n=41). Throughout the interface, TCR displaces LFA-1:ICAM-1 complexes to occupy the most central position available. Images were taken using epifluorescence microscopy.

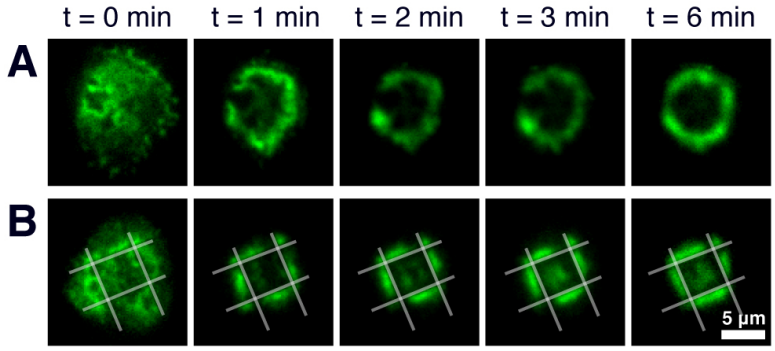

Figure 2.4: LFA-1 moves inward during IS formation. **(A)** LFA-1 labeled with anti-LFA-1 antibody (Alexa Fluor 488) forms a ring in T cells interacting with a freely diffusing SLB. **(B)** T cells presented with an SLB constrained by metal grid lines result in LFA-1 accumulation in areas within the corrals that are closest to the synaptic center. Images were taken using TIRF microscopy and the supported bilayers display GPI-anchored peptide-MHC and ICAM-1. The use of GPI-anchored proteins are less ideal for clustering studies due to apparently unavoidable clustering of these proteins in supported membranes as a result of the purification and reconstitution process.

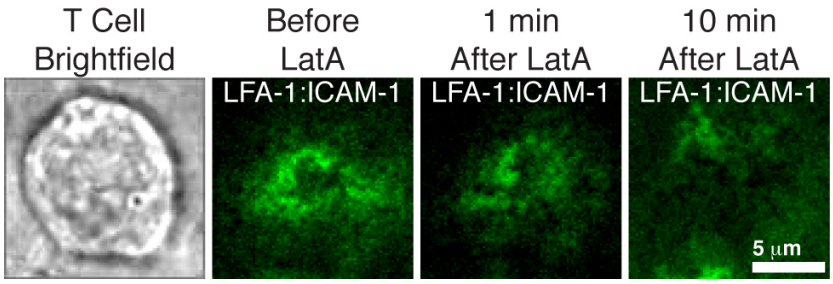

Figure 2.5: Disruption of actin polymerization with Latrunculin A dissolves the LFA-1:ICAM-1 ring.

2.3.3 TCR-pMHC microclusters exclude and displace LFA-1:ICAM-1 complexes

Simultaneous imaging of TCR and ICAM-1 reveals exclusion of LFA-1:ICAM-1 complexes by TCR microclusters. Upon initial cell contact with the bilayer, ICAM-1 begins to accumulate and TCR assembles into microclusters at the interface (Fig. 2.6, 1st column, A-C; observed in 90% of cells, n=44). After 5 minutes of cell interaction with the bilayer, 67% of the cells (n=122) contain voids (<300 nm in diameter) within the ICAM-1 ring that colocalize with the TCR:pMHC microclusters (Fig. 2.6, 2nd column, A-C and magnified images Fig. 2.6D). The ICAM-1 density within these voids is comparable to bulk density, indicating that unligated ICAM-1 is free to diffuse throughout the interface while LFA-1:ICAM-1 complexes are specifically excluded. Nascent TCR:pMHC microclusters continue to colocalize with the voids in the LFA-1:ICAM-1 ring after 15 minutes (Fig. 2.6, 3rd column, A-C) of cell interaction with the SLB (observed in 77% of cells, n=196).

LFA-1 and TCR do not translocate together although both are transported inward in an actin-dependent manner. Moreover, time-lapse images of TCR microclusters, shown as dark voids moving through the green LFA-1:ICAM-1 ring (Fig. 2.7A), reveal the competition between the different cluster sizes. The larger TCR:pMHC microclusters efficiently displace LFA-1:ICAM-1 complexes within the relatively static pSMAC. In addition to this dynamic displacement, we observe a static exclusion and spatial sorting between these proteins within peripheral regions of the synapse when substrate barriers block further inward transport (Fig 2.7B). Note how TCR:pMHC microclusters out-compete LFA-1:ICAM-1 complexes for the innermost positions within each corralled zone (observed in 66% of cells, n=101). Below we show a similar observation for differentially clustered, ligated LFA-1 (Fig. 5G). An important corollary of this observation is that segregation between the pSMAC and cSMAC is not driven exclusively by an internal difference in cellular structure between these two regions. From these observations, we conclude that an active differential sorting mechanism capable of distinguishing between TCR:pMHC microclusters and LFA-1:ICAM-1 complexes exists throughout the synaptic interface.

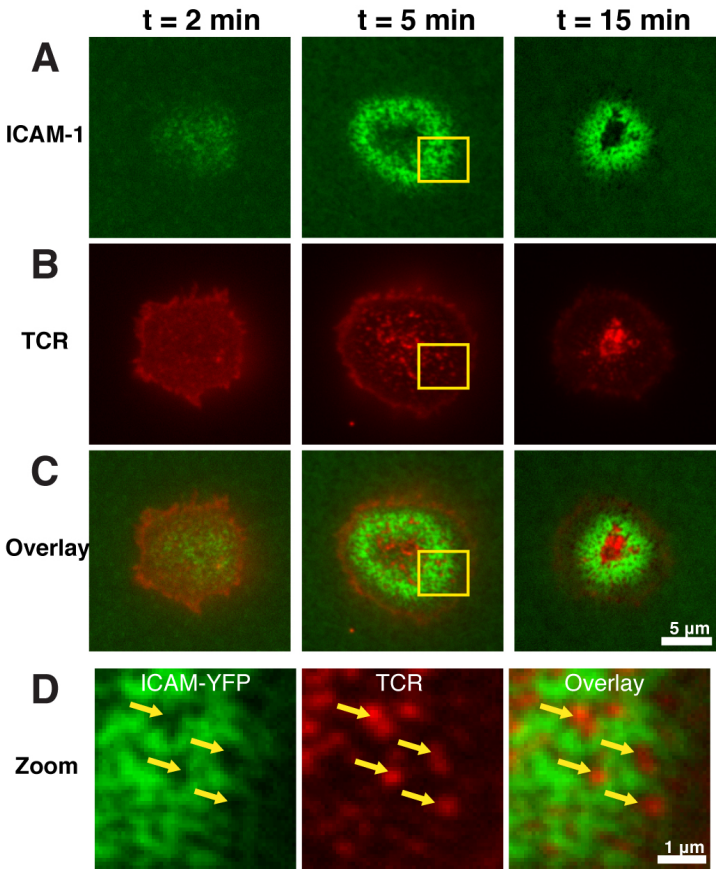

Figure 2.6: TCR microclusters exclude and displace LFA-1:ICAM-1 complexes. Epifluorescence images of ICAM-YFP **(A)** and T cells labeled with labeled aTCR-f_{ab} (Alexa Fluor 568) **(B)** that were fixed 2 min (1st column), 5 min (2nd column), and 15 min (3rd column) after contact with SLBs containing ICAM-1 and pMHC. Upon formation, TCR microclusters exclude and displace ICAM-1 as they translocate to the cSMAC. The ICAM-1 density within the excluded areas is comparable to the bulk density. **(C)** Composite image of ICAM-1 from (A) and TCR from (B). **(D)** Magnified images of the area indicated in (C) of the T cell fixed after 5 min.

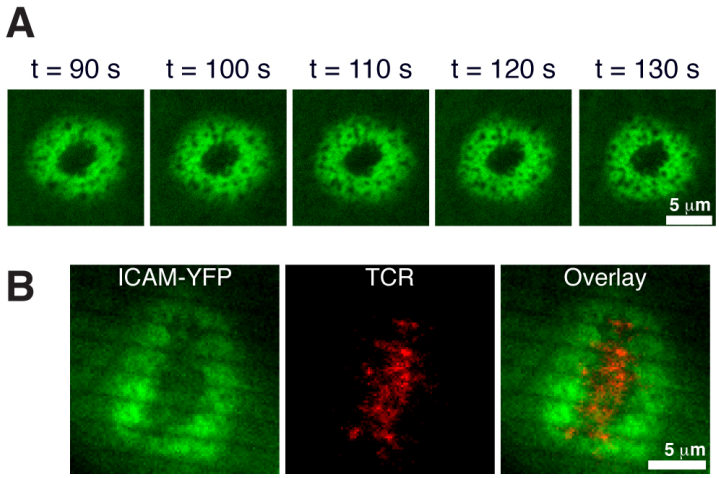

Figure 2.7: (A) Time-lapse images of TCR microclusters that appear as voids translocating through LFA-1:ICAM-1 complexes in the pSMAC of a mature synapse. **(B)** Fluorescent images taken with TIRF illumination of ICAM-YFP and TCR on live T cells exposed to a bilayer constrained by diffusion barriers (parallel lines with 2 mm spacing). Within the pSMAC, TCR:pMHC microclusters occupy the most central positions and exclude LFA-1:ICAM-1 complexes.

2.3.4 Cluster size determines LFA-1 spatial sorting in the IS

We manipulate the cluster size of LFA-1 to determine its effect on LFA-1 transport and radial distribution. LFA-1 distribution at the pSMAC is typically observed using the non-crosslinking H155 f_{ab} fragments (αLFA-f_{ab}), which are monovalent and lack the f_c portion (Fig. 2.4) [40,59]. Crosslinking LFA-1 with the H155 bivalent antibody (αLFA-mAb) increases its cluster size (Bi-X LFA-1). The αLFA-mAb may be crosslinked itself by a secondary antibody (αmAb), which specifically binds to the f_c portion. T cell incubation with this tetravalent crosslinker further increases the degree of LFA-1 clustering (Tetra-X LFA-1).

Cluster size-based protein sorting is observed by simultaneously labeling LFA-1 with f_{ab} fragments (No-X LFA-1) and either the bivalent or tetravalent crosslinker (Fig. 2.8A). Prior to interaction with the SLB, live T cells were concurrently incubated with fluorescently labeled H155 αLFA-mAb and αLFA-f_{ab}. No-X LFA-1 displayed the native broad annular pattern at the pSMAC. Bi-X LFA-1 also sorted into the pSMAC. However, the Bi-X LFA-1 clusters were transported further inward, leading to an enriched ring pattern in the inner zone of the pSMAC (Fig. 2.8B). Tetra-X LFA-1 localized in the cSMAC, where TCR:pMHC microclusters are recruited (Fig. 2.8C). Labeling with the different crosslinkers in the absence of LFA-1 preclustering did not result in the observed differences in LFA-1 spatial patterns (Fig. 2.9). These control experiments demonstrate that the spatial patterns are not the result of antibody binding affinity or protein accessibility issues.

The differential sorting can be quantified for a population of cells by generating averaged protein density plots of the normalized and azimuthally integrated intensities obtained for the various forms of LFA-1 as a function of the normalized cell radii (Fig. 2.8D inset). These averaged radial profiles (n=53 cells each) of the Bi-X LFA-1 (Fig. 2.8D) and Tetra-X LFA-1 (Fig. 2.8E), compared to the radial profile of No-X LFA-1, reveal the different characteristic spatial sorting as a function of cluster size. The mean normalized radii at which peak intensities (maximum protein concentrations) occur for each case (±SE) are clearly different with the more inward positions occupied by the more highly crosslinked species (p value<0.001 for both sets, Student's t test). Slight differences between the mean radial positions at peak intensities for the No-X LFA-1 may occur due to No-X LFA-1 exclusion from the inner pSMAC zone by the Bi-X LFA-1.

The overall synapse morphologies of ICAM-1 (pSMAC) and TCR (cSMAC) are largely unaffected by the induced clustering of a sub-population of LFA-1 in these experiments (Fig. 2.8F). The unaltered distribution of ICAM-1 at the pSMAC for all degrees of crosslinking (Fig. 2.10B and 2.10C) applied indicates that a sufficient population of non-crosslinked and unlabeled ligated LFA-1 is present to preserve the broad pSMAC pattern. Direct crosslinking of LFA-1 may preferentially sort unligated LFA-1 to the cSMAC given that ICAM-1 accumulation, which maps only ligated LFA-1, does not reflect the distributions of crosslinked LFA-1 at the IS.

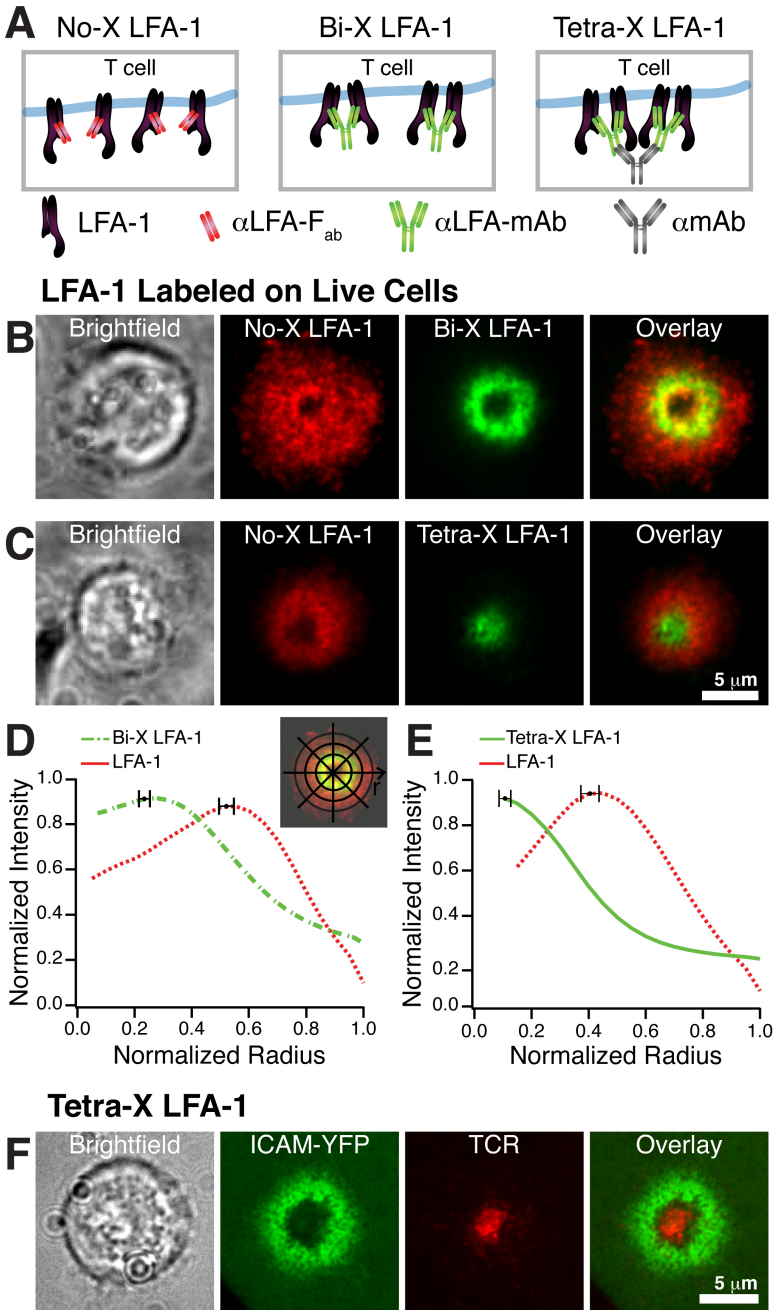

Figure 2.8: Increased clustering of LFA-1 changes its spatial localization. LFA-1 was labeled in live cells (B, C, H) or fixed (F, G) cells and imaged with TIRF microscopy. **(A)** Diagram of the degrees of LFA-1 clustering. **(B)** T cells were labeled with H155 aLFA-f_{ab} fragment (No-X LFA-1) and aLFA-mAb (Bi-X LFA-1). **(C)** H155 aLFA-mAb was preclustered by crosslinking with an antibody (amAb) and T cells were labeled as in (B) to give No-X LFA-1 and Tetra-X LFA-1. Averaged radial profile plots (n=53 cells each) of intensities as a function of the normalized cell radii obtained for Bi-X LFA-1 **(D)** and Tetra-X LFA-1 **(E)** compared to No-X LFA-1. **(Inset)** The integrated intensity is the sum of the pixel values along each circle at a given radius and is normalized by the number of pixels in the circle. The mean peak intensities (±SE) are shown (p value<0.001 with the Student's t test). Data are representative of three independent experiments. **(F)** For T cells incubated with the tetravalent crosslinker, the ICAM-1 ring and TCR central cluster is maintained. Thus, ICAM-1 and TCR synapse morphology is unaffected by crosslinking a subpopulation of cell-surface LFA-1.

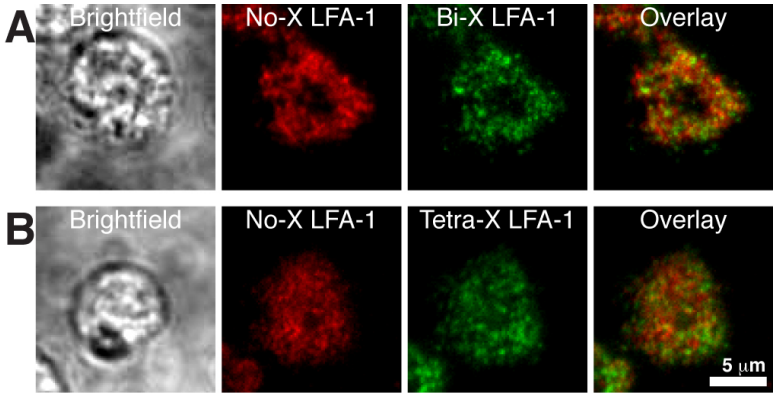

Figure 2.9: Preclustering of LFA-1, not simply antibody labeling, is necessary for changes in LFA-1 spatial pattern. Live T cells were incubated with the SLB for 10 minutes, fixed with paraformaldehyde, and labeled with the anti-LFA-1 antibodies after membrane permeabilization with detergent. LFA-1 displays the same distribution in the pSMAC regardless of whether the antibody label was the monovalent **(A and B, red)**, bivalent **(A, green)**, or tetravalent crosslinking agent **(B, green)**.

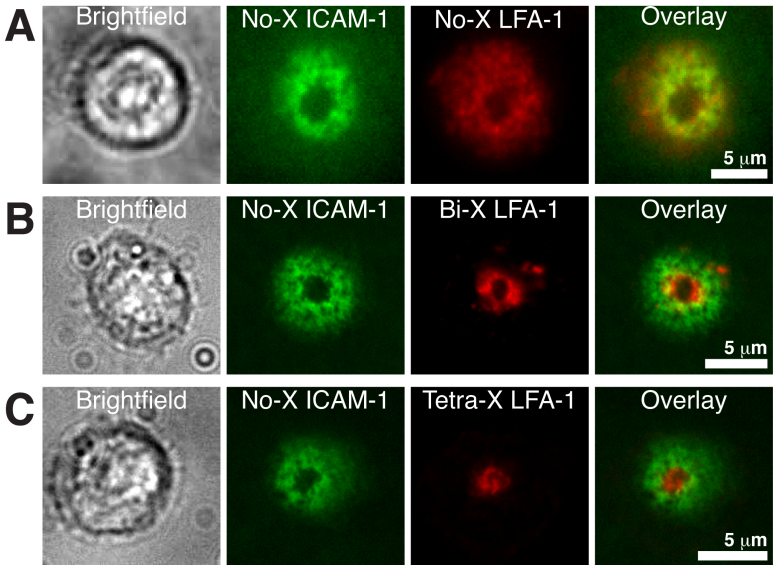

Figure 2.10: **(A)** LFA-1 labeled with H155 f_{ab} fragment colocalizes with ICAM-YFP at the pSMAC. **(B)** Bi-X LFA-1 forms a narrow ring in the inner zone of the pSMAC and ICAM-YFP forms the typical broad ring pattern at the pSMAC. **(C)** Tetra-X LFA-1 forms a central cluster at the cSMAC and the ICAM-YFP pattern is unaltered as before.

2.3.5 Crosslinked ICAM-1 increases inward transport of active LFA-1

In order to selectively study crosslinking effects on LFA-1 ligated to ICAM-1, we utilize a bivalent crosslinking antibody against the YFP domain (aYFP-mAb) of the ICAM-1-YFP fusion protein. Targeting the YFP moiety precludes any allosteric or blocking effect that antibody binding may have on the LFA-1 binding site on ICAM-1. This indirect crosslinking strategy allows us to selectively induce crosslinking of LFA-1:ICAM-1 complexes. Crosslinked ICAM-1 (Bi-X ICAM-1) is formed by incubation of the bilayer containing ICAM-YFP and pMHC with aYFP-mAb before T cell addition (Fig. 5A). The different spatial distributions of LFA-1:ICAM-1 complexes, as a function of ICAM-1 crosslinking, are evident in the quantitative fluorescence images presented in Figure 2.11. These images are calibrated to reveal absolute protein densities using a method based on supported bilayer standards [64]. Imaging the fluorescently labeled aYFP-mAb responsible for crosslinking the ICAM-YFP reveals that it is primarily concentrated in the cSMAC (Fig. 2.11C, right). Linescans of protein densities along the dashed lines on figures 2.11B and 2.11C are also shown (Fig. 2.11D). An ICAM-1:aYFP-mAb ratio greater than 2:1 requires that additional ICAM-1 be indirectly linked through LFA-1 linkages in the T cell. The roughly 6:1 ICAM-YFP:aYFP-mAb ratio observed in the cSMAC (Fig. 2.11D, inset) provides evidence for native LFA-1 organization into pre-existing clusters of not more than a few molecules [54,57]. These observations indicate that LFA-1:ICAM-1 complexes, which have been crosslinked through ICAM-1, preferentially segregate closer to the cSMAC while non-crosslinked LFA-1:ICAM-1 complexes primarily populate the pSMAC. The use of a tetravalent crosslinker against ICAM-1 (Tetra-X ICAM-1) results in complete transport of ICAM-1 to the cSMAC (Fig. 2.11A). The average radial profiles of tetra-X ICAM-1 and TCR with mean peak integrated intensities (±SE) further confirm the colocalization of LFA-1:Tetra-X ICAM-1 and TCR at the cSMAC (Fig. 2.11B).

To ensure that we are not drastically changing cell signaling and, in effect, actin polymerization and transport of the LFA-1:ICAM-1 complexes, we measure cytosolic calcium levels. Time course experiments to monitor changes in the Ca^{2+} levels were done from 0-20 minutes after cell interaction with the bilayer. The resulting curves do not show any difference in the strength or pattern of Ca^{2+} activation between non-crosslinked T cells (Fig. 2.12A) and cells with LFA-1:Tetra-X ICAM-1 clusters (Fig. 2.12B). All curves for each experiment were subsequently integrated from 1-20 minutes and plotted as shown in Figure 2.12C to clearly indicate that additional clustering of LFA-1 does not does not lead to differences in cell signaling between cells interacting with Tetra-X ICAM-1 and cells forming native patterns. Addition of Latrunculin A to T cells interacting with these differently crosslinked ICAM-1 species result in synaptic patterns that are not well resolved (Fig. 2.13). Therefore, larger LFA-1:ICAM-1 clusters still depend on the actin cytoskeleton to maintain the spatial patterns.

Protein sorting between crosslinked and non-crosslinked ICAM-1 can be directly observed when both populations simultaneously interact with a T cell. Bilayers containing pMHC, fluorescently labeled ICAM-1 (Alexa-Fluor 647) lacking the YFP moiety (No-X ICAM-1), and ICAM-YFP (Bi-X ICAM-1) are incubated with aYFP-mAb before T cell addition. Upon T cell activation, the Bi-X ICAM-1 can be seen to segregate from the No-X ICAM-1 (Fig. 2.14A). The more centrally biased distribution of LFA-1:Bi-X ICAM-1 relative to the LFA-1:No-X ICAM-1 is also evident in the cell population averaged radial profiles (Fig. 2.14B n=63, mean±SE). No-X ICAM-1 fluorescence intensities in the cSMAC are comparable to bulk intensity values, indicating free diffusion of unligated ICAM-1 throughout the synaptic junction. When the same bilayer system is constrained into patterned grid arrays of diffusion barriers, LFA-1:Bi-X ICAM-1 complexes clearly occupy the most radially inward positions along the barriers and exclude LFA-1:No-X ICAM-1 complexes (Fig. 2.14C). Crosslinking alters the clustering state of ligated LFA-1, and the cell transports crosslinked LFA-1:ICAM-1 complexes further inward than non-crosslinked ICAM-1. This recapitulates the sorting phenomenon we previously observed between native LFA-1:ICAM-1 complexes and TCR microclusters (Fig. 2.7B).

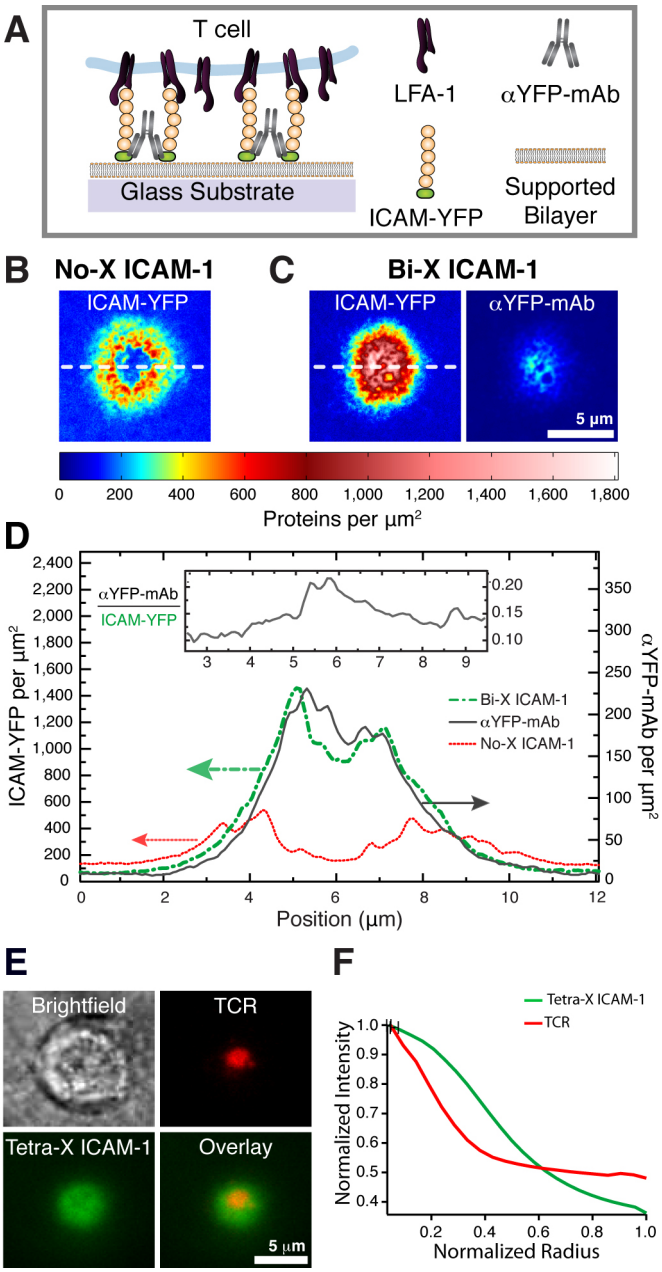

Figure 2.11: Crosslinking ICAM-1 alters synapse morphology. **(A)** Diagram of ICAM-YFP crosslinked with aYFP-mAb (Bi-X ICAM-1). **(B)** Quantitative protein density map of ICAM-YFP in a native synapse and **(C)** ICAM-YFP and aYFP-mAb (Alexa-Fluor 568) in a synapse with Bi-X ICAM-1. Images were taken by epifluorescence microscopy. **(D)** Linescans through the center of each cell plot ICAM-YFP density (left axis) and aYFP-mAb density (right axis). **(Inset)** Plot of aYFP-mAb/ICAM-YFP using linescan values for areas within the cell. **(E)** aYFP-mAb was incubated with a secondary antibody prior to bilayer incubation to form tetravalent crosslinkers. ICAM-1 crosslinked with a tetravalent crosslinker (Tetra-X ICAM-1) forms a central cluster and colocalizes with TCR at the cSMAC. The larger size of the LFA-1:Tetra-X ICAM-1 central cluster compared to the TCR:pMHC cluster may be due to the presence of various degrees of ICAM-1 crosslinking possible with the tetravalent crosslinker. **(F)** Average radial profiles of tetra-X ICAM-1 and TCR with mean peak integrated intensities (±SE) are shown and obtained as in Fig 2.8.

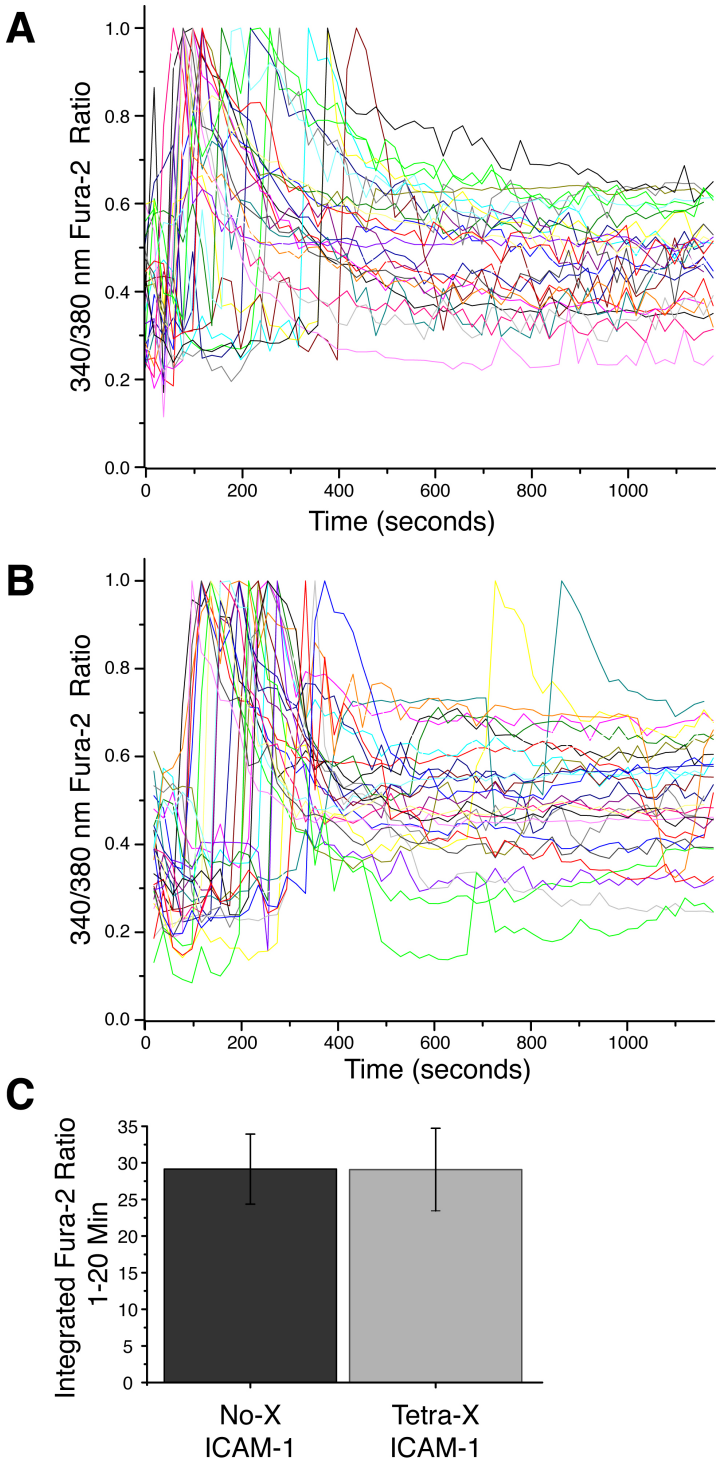

Figure 2.12: Changes in the spatial pattern of LFA-1:ICAM-1 complexes do not alter T cell Ca^{2+} signaling. **(A)** Changes in cytosolic calcium levels were measured using Fura-2 ratiometric dye for T cells interacting with a bilayer displaying pMHC and No-X ICAM-1. **(B)** Measurement of Ca^{2+} signaling for T cells interacting with the highly crosslinked tetra-X ICAM-1 species. Measurements were taken from 0-20 minutes. **(C)** Mean integrated Fura-2 ratio (±SE) for **(A)** and **(B)** (n=26, 27 respectively).

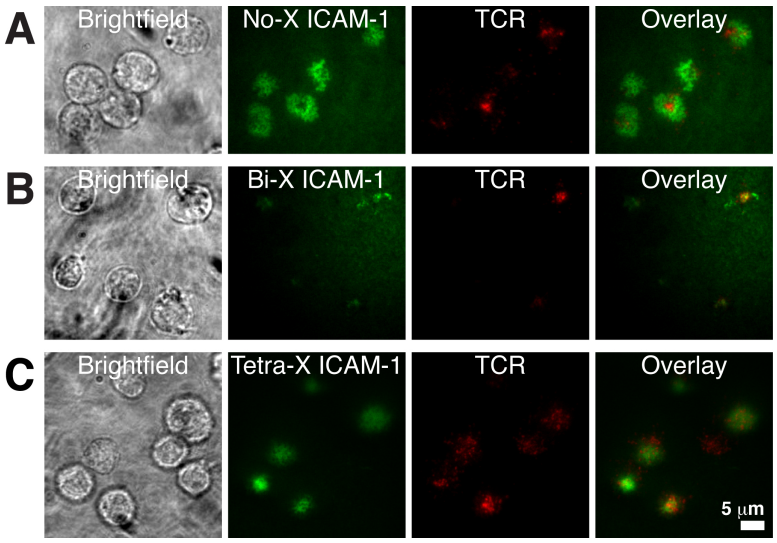

Figure 2.13: **(A)** Addition of Latrunculin A one minute following T cell interaction with the bilayer leads to distorted ICAM-1 and TCR patterns. Latrunculin A was also added to T cells within 1 minute of exposure to bilayers displaying bi-X ICAM-1 **(B)** and tetra-X ICAM-1 **(C)**.

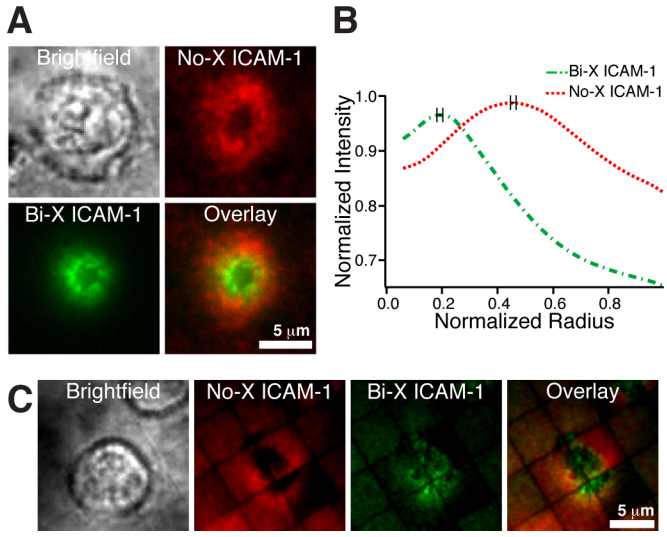

Figure 2.14: **(A)** Bi-X ICAM-1 and non-crosslinked ICAM-1 (No-X ICAM-1) are simultaneously presented on the bilayer prior to T cell addition **(B)** Average radial profiles of No-X ICAM-1 and Bi-X ICAM-1 with mean peak integrated intensity (±SE) are shown and obtained as in Figs. 2.8 and 2.11 (p value<0.001 with the Student's t test). Data are representative of five independent experiments. **(C)** Bi-X ICAM-1 and No-X ICAM-1 sorting are also shown for when the bilayer is corralled by 5 mm x 5 mm grid squares. As seen with TCR and ICAM-1, Bi-X ICAM-1 occupies the most radially inward positions along the grid lines within the pSMAC, displacing No-X ICAM-1.

2.4 Discussion

Upon T cell activation, LFA-1 and TCR engage their ligands and become sorted into the pSMAC and cSMAC by radial transport within the T cell-APC junction. Direct or indirect external crosslinking of LFA-1 on T cells preceding IS formation alters its spatial sorting. Specifically, we have observed a graduated response in which a bivalent crosslinker redirects LFA-1:ICAM-1 complexes to the innermost radii of the pSMAC while a tetravalent crosslinker causes them to localize in the cSMAC. These results indicate that the crosslinking state of LFA-1 can determine its final position within the IS.

We propose a mechanistic model whereby the sorting of proteins results from differential strengths of coupling to the moving actin cytoskeletal network. Linking of cell surface proteins to actin (e.g. via talin, ezrin or other less direct methods) may be described as frictional coupling (24, 25). The result is that a protein, or cluster of proteins, on the cell surface experiences a driving force in the direction of actin cytoskeletal flow. If individual bonds form and break rapidly, then it is not necessary that the proteins be driven at the same speed, or even in the same direction as the actin flow. Indeed, it has been previously reported that TCR clusters can be driven at angles to the preferred flow when they encounter physical barriers [51]. If we speculate that the strength of coupling to the cytoskeleton exhibits a nonlinear scaling with protein density (e.g. there is a degree of cooperative binding), then the result is a cluster size mediated sorting of the type observed in the experiments described here.

Under such a mechanism, all proteins in the membrane will experience a driving force determined by the composite of their specific coupling chemistry to the actin network and their local clustering state. The transport progresses until a quasi-equilibrium radial distribution is reached in which the inward driving force of each protein cluster species is balanced by local competition from surrounding clusters. This is analogous to sedimentation equilibrium, in which denser species out-compete less dense species for the down-field positions in a force field (e.g. centrifugal, gravitational, electric, etc.) [65,66]. In the case of the T cell IS, the driving force is the actin cytoskeletal flow and the coupling force per unit area experienced by the protein clusters determines their relative positions. TCR clusters clearly have a higher coupling force density than native LFA-1:ICAM-1 complexes. This conclusion is partly based on our observations of the ability of TCR clusters to physically displace LFA-1:ICAM-1 *en route* to the cSMAC (Fig. 2.7). Additionally, TCR trapped in the pSMAC region on patterned substrates displace LFA-1 from the innermost radial positions of each corral (see Fig. 2.3B and Fig. 2.7B). For the same reasons, TCR clusters, along with other cSMAC localizing proteins, such as CD28:B7-1 [67] (Fig. 2.16), could prevent the more weakly coupled LFA-1 from entering the cSMAC (Fig. 2.15A). External crosslinking of LFA-1 into larger clusters increases the coupling force density, enabling LFA-1 clusters to effectively compete with TCR for cSMAC territory (Fig. 2.15B and 2.15C). The mechanism we suggest here is consistent with all of the observations discussed. However, other mechanisms have also been proposed.

Size exclusion and membrane bending effects have long been considered as possible contributors to protein sorting within the IS [15,68,69,70]. It has been suggested that the larger ectodomain of LFA-1:ICAM-1 complexes (~42 nm) prevent their colocalization with TCR:pMHC complexes (~15 nm) at the cSMAC. Observation of LFA-1:Tetra-X ICAM-1 clusters in the cSMAC suggests that size exclusion alone is insufficient to define cSMAC composition. Additionally, topographic imaging of this altered cSMAC region by reflection interference contrast microscopy (RICM) indicates that membrane topography conforms to the interleaved protein composition (Fig. 2.15D and E). Although size exclusion may be a factor in protein segregation over shorter length scales, it is not the primary force behind cSMAC formation. Indeed, size exclusion is not sufficient to prevent LFA-1:ICAM-1 complexes from entering the cSMAC when the actin cytoskeleton drives them there. A more recently proposed hypothesis suggests that cluster stability may contribute a differentiating characteristic that targets LFA-1 and TCR to the pSMAC and cSMAC, respectively [30]. In this model, sorting occurs because LFA-1 clusters need actin for stability but TCR clusters do not, allowing TCR to enter the actin-deficient cSMAC while LFA-1 cannot. Our observation of externally cross-linked LFA-1 entering the cSMAC is consistent with this hypothesis. However, the

additional stratification and exclusion we observe of non-crosslinked, active LFA-1 by the species coupled to a bivalent crosslinker within the pSMAC is more difficult to account for based on cluster stability alone (Fig. 5H). We thus conclude that, while cluster stability will certainly contribute to spatial sorting, differential stability is not required for sorting. The predominant discrimination mechanism operating over most of the synaptic junction appears to be based on overall strength of protein coupling to actin. A compelling feature of the relatively simple frictional coupling mechanism is the ease with which it could be utilized by all proteins within the IS.

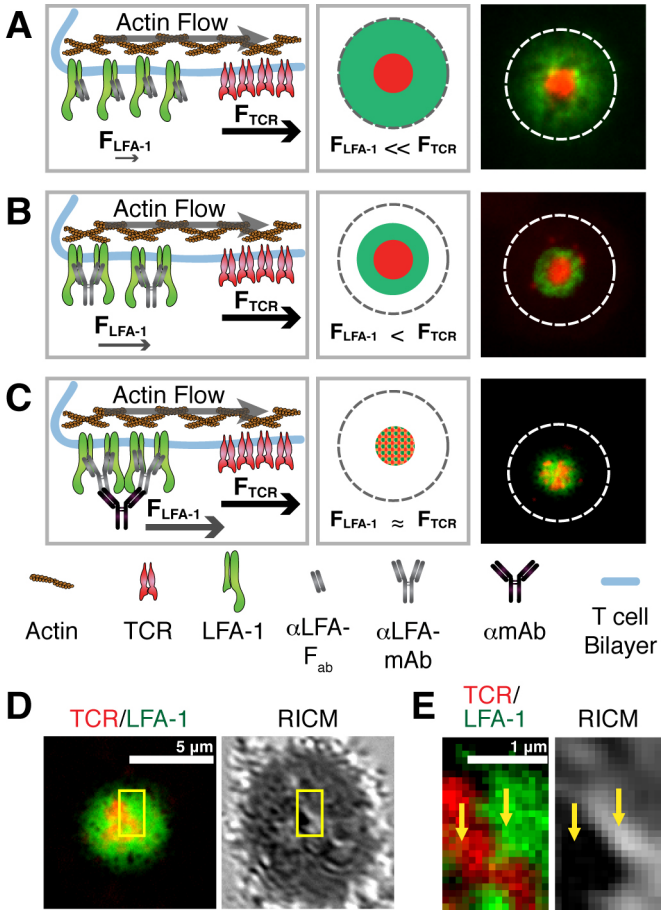

Figure 2.15: Schematic of the model for protein sorting in IS formation. LFA-1 and TCR transport are coupled to actin centripetal flow and the strength of actin attachment scales with the protein cluster size. **(A)** Microclusters of TCR and relatively non-clustered LFA-1 molecules are transported inward and TCR forms a central cluster in the cSMAC surrounded by a ring of LFA-1 in the pSMAC. **(B)** Crosslinking of LFA-1 with a bivalent crosslinker increases its coupling to actin, resulting in LFA-1 accumulation in the inner zone of the pSMAC. **(C)** Crosslinking LFA-1 with a tetravalent crosslinker forms large LFA-1 clusters, leading to comparable coupling strengths of LFA-1 and TCR to actin. Both TCR and LFA-1 occupy the cSMAC. **(D)** Fluorescence images of the small-scale segregation between TCR:pMHC (red) and LFA-1:ICAM-1 (green) complexes in the cSMAC. The RICM image reveals membrane topography and darker areas indicate closer membrane interactions. **(E)** Magnified fluorescence and RICM images of the area indicated in (D). TCR:pMHC complexes colocalize with darker regions in the RICM and LFA-1:ICAM-1 complexes colocalize with the lighter regions.

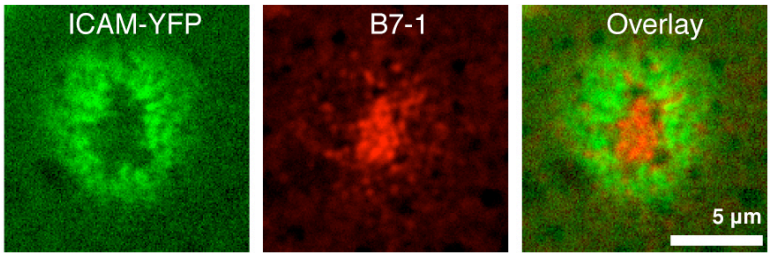

Figure 2.16: B7-1 forms microclusters and are transported to the cSMAC during IS formation. T cells were presented to the SLB displaying histidine-tagged ICAM-YFP, pMHC, and B7-1. After 10 minutes of interaction, cells were fixed with paraformaldehyde and imaged using epifluorescence microscopy. B7-1 **(red)** is present as a central cluster at the cSMAC and as microclusters that do not colocalize with ICAM-1 **(green)** in the pSMAC.

2.5 Experimental Procedures

2.5.1 Cells and Reagents

Primary naïve T cells harvested from splenocytes of first generation AND x B10.BR transgenic mice from Jackson Laboratory (Bar Harbor, Maine) were expanded to $CD4^+$ T cell blasts and maintained as described [36,51]. This protocol is approved by the Animal Welfare and Research Committee (AWRC) under Animal Use Protocol #17702. All lipids were obtained from Avanti Polar Lipids (Alabaster, AL). Full length and f_{ab} fragments of H155 anti-LFA-1 and H57 anti-TCR antibodies were prepared by standard protocols. Mouse 3E6 anti-GFP antibody that cross-reacts with YFP, secondary antibodies Alexa Flour labeling kits, and purification columns were obtained from Invitrogen (Carlsbad, CA). MCC peptide (88-103, ANERADLIAYKQATK) was obtained from Biosynthesis, Inc. (Lewisville TX) AND Dana-Farber Core Facility (Boston, MA). Histidine-tagged ICAM-1, ICAM-1-YFP fusion protein and MHC Class II I-E^K were expressed and purified as described [33]. Secreted ICAM-1 with a decahistidine tag at its C-terminus was expressed in Hi5 cells. The cells were retrovirally transfected from baculovirus (a gift from M. Davis) expressed in SF9 cells. Secreted MHC with a hexahistidine tag at the C-terminus of both a and b chains was expressed in S2 fly cells (a gift from L. Teyton and M. Davis). Cells were grown in Insect Xpress medium. Protein expression was induced by addition of 100 mM of $CuSO_4$. Protein was purified three days after transfection on an Agarose-Ni^+-NTA affinity column with an imidazole gradient and stored at -80°C in Tris buffer with 10% glycerol until use.

2.5.2 Patterned Substrates

Coverslips patterned with metal lines were made as previously described [36,51] and used as the bottom face of a temperature controlled flow cell chamber (Bioptechs, Butler, PA). Metal lines were roughly 100 nm in width and 5.5 nm in height. All substrates were etched in piranha solution (3:1 H_2SO_4:H_2O_2), rinsed copiously with H_2O, and dried under a stream of N_2 gas.

2.5.3 Supported Membrane

Moth cytochrome *c* (MCC) peptide was loaded into the MHC by overnight incubation at a final concentration of 100 mM at 37°C in pH 4.5 citrate buffer. DOPC bilayers comprised of 2 mol% Ni^{2+}-NTA-DOGS were prepared by standard methods. Supported bilayers were subsequently incubated with ICAM-1 and MHC for an hour in Tris buffer. The flow cell was heated to 37°C and rinsed with 10 mL buffer prior to the addition of live murine AND CD^{4+} T cells. For experiments with the bivalent crosslinker against ICAM-1, mouse 3E6 full antibody (aYFP-mAb) was added to the heated

flow cell at 5 mg/mL and incubated for 20 minutes prior to cell addition. When the tetravalent crosslinker was used, the aYFP-mAb was incubated with 4 mg/mL of goat anti-mouse antibody prior to bilayer incubation.

2.5.4 Imaging

In live cell experiments, the nonblocking antibodies H155 aLFA-mAb (Alexa Fluor-488), H155 aLFA-f_{ab} (Alexa Fluor-568), and H57 aTCR-f_{ab} (Alexa Fluor-568) were incubated with the cells at 5 mg/mL for 20 min at 4°C in isotonic conditions as indicated. For experiments using the tetravalent crosslinker against LFA-1, H155 aLFA-mAb was preincubated with goat anti-rat antibody at 5 mg/mL prior to cell incubation. Cells were then injected into a 37°C closed cell chamber and imaged immediately. For fixed cell experiments, unlabeled cells were first injected into the 37°C closed cell chamber and allowed to interact with the supported membrane for the indicated time. Cells were then fixed with 2% paraformaldehyde, permeabilized with 0.05% Triton-X, blocked with 5% casein, and labeled with indicated antibodies at room temperature.

For TIRF microscopy, images were acquired on a Nikon TE2000 inverted microscope with a 100x 1.49NA oil immersion TIRF objective. Data were acquired with the MetaMorph software package (Molecular Devices) and a Cascade 512B EMCCD camera (Roper). RICM and epifluorescence images were taken on Nikon TE300 inverted microscope with a 100x 1.3 NA oil immersion objective. Data were acquired with Metamorph software package and a CoolSnapHQ Camera (Photometrics). Radial profile analysis was performed using the radial profile plugin for ImageJ software.

Chapter 3

Size-Based Sorting of LFA-1:ICAM-1 Clusters at the Immunological Synapse

3.1 Abstract

In the previous chapter, we discussed how changing the cluster size of LFA-1:ICAM-1 complexes drastically changes its spatial distribution. Our results demonstrate that cluster size is a critical parameter in determining protein spatial positioning in the IS. We propose a sorting mechanism based on frictional protein coupling to the actin cytoskeleton to explain our results. In this chapter, we follow up on our observations and determine to what extent the LFA-1:ICAM-1 complexes are clustered and, more importantly, how these clusters are organized in the native IS. We collect fluorescence fluctuation measurements of ICAM-YFP molecules moving within a small laser excitation area—less than 1/100th of the typical area of the IS. This affords exquisite spatial precision and allows us to sample many areas in the pSMAC. We discover that two populations of LFA-1:ICAM-1 complexes exist—small oligomers and larger clusters that are quickly bleached in the laser spot. Finally, we confirm the existence of a gradient of LFA-1:ICAM-1 cluster sizes across the pSMAC, as predicted by the frictional force-coupling model. Finally, we discuss future work to determine the number of molecules within these clusters and the dependence of the cluster size gradient on the actin cytoskeleton.

3.2 Introduction

Intercellular communication and cell signaling requires the spatial and temporal organization of proteins, lipids, and other molecules at cell membranes [71]. The two-dimensional and fluid nature of membranes, in addition to interactions with cytoskeletal elements, makes them ideal scaffolds for signaling events. Although the membrane's role in signaling is becoming known, the theoretical underpinning of how it orchestrates organization at various length scales is largely unknown. One well-studied example of this is the formation of the immunological synapse (IS)—the first step in mounting an immune response [20]. The IS, which forms between a T cell and an antigen presenting cell (APC), exemplifies how protein spatial organization can modulate cell triggering [72]. Within this intercellular structure, membrane receptor-ligand pairs become arranged into concentric domains of signaling molecules, classically called supramolecular activation clusters (SMACs). The main signaling complex, the T cell receptor (TCR) bound to major histocompatibility complex displaying a specific antigenic peptide (pMHC), resides in the central SMAC or cSMAC. Beyond this is the peripheral SMAC (pSMAC) occupied by the adhesion molecule lymphocyte function associated antigen 1 (LFA-1) bound to its intercellular adhesion molecule-1 (ICAM-1) ligand. Finally, the outermost ring, called the distal SMAC (dSMAC), contains large glycoproteins lacking cognate ligands on the APC, such as CD44, CD45, and CD46 [73].

Early studies with pharmacological inhibitors that targeted the cytoskeleton led to the discovery that IS formation depended on actin transport [21,30]. Furthermore, it was also believed that disparities in the ectodomain sizes of TCR-pMHC (~14 nm) and LFA-1:ICAM-1 (~42 nm) complexes led to protein sorting at the IS. This configuration allowed for the minimization of stress induced by membrane bending [15]. However, later studies suggest that protein sorting may ultimately be driven by protein cluster size instead of receptor-ligand ectodomain sizes [74].

Preceding IS formation, TCR:pMHC complexes form smaller clusters ~300 nm in diameter, which are easily detected by fluorescence microscopy [50]. The nucleation and radial transport of these microclusters are actin-dependent. Other costimulatory molecules, such as CD28:B7-1 [67] and CD2:CD58 complexes also form microclusters and are shuttled to the cSMAC as well [75]. Whereas these complexes are highly clustered prior to transport, LFA-1 does not cluster to the same extent upon binding its ICAM-1 ligand. Recently, we demonstrated that protein cluster size prior to centripetal transport determines their spatial localization [74]. We increase the cluster sizes of LFA-1:ICAM-1 complexes two additional degrees with antibody crosslinking and observe a corresponding change in the resulting LFA-1:ICAM-1 patterns. A bivalent crosslinker results in a smaller LFA-

1:ICAM-1 ring at the pSMAC and a tetravalent crosslinker leads to a central cluster of LFA-1:ICAM-1 complexes at the cSMAC. Although both LFA-1:ICAM-1 and TCR-pMHC clusters occupy the cSMAC, they remain in distinct domains and the membrane bends to accommodate the interleaved configuration [74].

Based on our results, we propose a frictional force coupling model to describe the mechanism of IS formation. In this model, protein cluster size is nonlinearly related to the degree of coupling to and transport by the actin cytoskeleton. The ability of LFA-1:ICAM-1 clusters to compete for cSMAC territory indicates that active transport by actin can supersede more passive processes such as thermodynamic restrictions on membrane bending. Another cluster-based model points to the differential stability of the clusters in the different SMACs and molecular crowding at the cSMAC as the reasons for differential protein sorting. However, this model does not account for the differential patterns in the pSMAC and the ability of LFA-1:ICAM-1 complexes to enter the cSMAC.

Here, we explore the cluster size-based protein sorting in the native IS. The frictional force coupling model predicts that a gradient of cluster sizes should exist across the pSMAC. Given that LFA-1:ICAM-1 clusters cannot be resolved with conventional fluorescence microscopy, we turned to fluorescence fluctuation analysis to detect dynamic protein clustering with spatial and temporal precision. First, we substitute a fluid supported lipid bilayer (SLB) displaying ICAM-1 and pMHC for the APC to optimize the imaging plane and reduce background signal. We scan across the IS with a 500 nm diameter laser spot and measure changes in the fluorescence fluctuations of LFA-1 bound, fluorescent ICAM-1-YFP molecules within the illuminated area. With each measurement, we observe immediate bleaching followed by persistent fluctuations in the ICAM-1-YFP signal. No bleaching is observed for similar measurements on areas of the bilayer that do not interact with a T cell. We interpreted the bleached component as the fraction of bound ICAM-1-YFP in large, slow moving clusters. In addition, we use the photon counting histogram (PCH) analysis to the fluorescent fluctuations and detect very small clusters of no more than 3 ICAM-1-YFP molecules. Our results indicate that two differently clustered populations of LFA-1:ICAM-1 complexes exist at the IS. Interestingly, the fraction of LFA-1:ICAM-1 complexes within the slower moving clusters increases toward the center. Thus, more compartmentalized domains beyond the classical SMACs exist at the IS and our results support the frictional force coupling model as the mechanism of IS formation.

3.3 Results

3.3.1 Detection of ICAM-YFP dimerization

We first determine whether fluorescent fluctuation analysis can accurately detect the oligomerization of the fusion protein ICAM-1-YFP. To do this, we analyzed the change in the clustering state of ICAM-1 due to crosslinking induced by an antibody specific to its YFP moiety. Fluorescent fluctuation measurements of ICAM-YFP were taken before (Figs. 1A, left & 1B) and after (Figs. 1A, right & 1C) antibody crosslinking on the SLB, which also displays pMHC. To crosslink ICAM-YFP, a buffered solution containing 5.7 μg/ml αYFP antibody was added and incubated with the SLB for 20 minutes prior to taking additional measurements. Fig. 1B and 1C show the raw data of intensity fluctuations as a function of time for non-crosslinked (red, Fig. 1B) and crosslinked (green, Fig. 1C) ICAM-YFP.

Two analytical methods may be used to analyze the fluorescence fluctuation measurements. The classical method is the generation of autocorrelation functions, which characterizes the average residence time and the average number of the molecules inside the excitation area. The crosslinked and non-crosslinked autocorrelation functions can then be fitted to theoretical functions describing two-dimensional free diffusion. This allows us to extrapolate the G(0) value, which is inversely proportional to the number of groups of ICAM-YFP in the excitation area, N_1 (Eq. 1).

(1) $$G(0) = \frac{1}{N_1}$$

To obtain the molecular brightness, B_1, of individual ICAM-YFP molecules, we divide the average fluorescence intensity within the excitation area by N_1.

To determine the degree of ICAM-YFP dimerization after the addition of the crosslinking antibody, we modify the *G(0)* to reflect the different species present. Specifically, the $G(0)$ value for multiple species, monomers and dimers in this case, is the sum of all single species $G(0)$ values weighted by the square of the molecular brightness, B_1 [76]:

(2) $$G(0) = \frac{B_1^2 N_1 + (2B_1)^2 N_2}{(B_1 N_1 + 2B_1 N_2)^2} = \frac{N_1 + 2^2 N_2}{(N_1 + 2N_2)^2}$$

Here we assume the brightness of crosslinked ICAM-YFP (dimer) is twice that of ICAM-YFP monomer [77]. N_1 and N_2 are the numbers of monomers and dimers, respectively. The total number of ICAM-1-YFP, N_{total} can be obtained by dividing the average fluorescence intensity of the measurement after crosslinking by B_1 from the measurement before crosslinking. Note that N_{total} is also equal to N_1+2N_2 (Eq. 3).

(3) $$N_{total} = N_1 + 2N_2$$

Combining equations (2) and (3), one can solve for the two unknowns N_1 and N_2 to determine the degree of dimerization (Eq. 4).

(4) $$Dimerization = \frac{2N_2}{N_{total}}$$

Using this brightness analysis, we determined that the surface density of ICAM-YFP was 320±12 /μm² before antibody crosslinking and the degree of dimerization was 37±3% after antibody crosslink. This means that 37% of the total ICAM-YFP population in the excitation area is in dimers.

The other analytical method that may be applied is the photon counting histogram (PCH) analysis developed by Gratton et al. [78,79]. This method measures the statistical amplitudes of molecular brightnesses within the focal area at any given time. It has been shown that the probability distribution of photon counts can be described by two parameters for each fluorescent species: the molecular brightness and the average number of molecules inside the excitation area. The PCH of multiple species is the successive convolution of the PCH of each individual species. The resulting histogram is typically characterized as super-Poissonian, since it still depends on fluctuations in amplitudes [78]. We first fitted the data obtained from a non-crosslinked sample with the single species model to determine the molecular brightness, B_1, of a single ICAM-YFP. The B_1 value was then used as a fixed parameter when we analyze the data from measurements taken after crosslinking using a two-species model (Fig. 1F). The PCH analysis yields a value of 35% for the degree of ICAM-1-YFP dimerization, in close agreement with the brightness analysis value. Previously, Gratton et al. found that the calculated number of fluorescent groups, N_1, within the excitation area by PCH analysis scaled more closely to the average photon counts than the *G(0)* analysis [78]. For the rest of the paper, fluorescent fluctuation measurements are taken of ICAM-YFP interacting with LFA-1 on the T cell surface, which can yield a more varied population of differently crosslinked species. Given that the PCH analysis more accurately reflects changes in the photon counts, forthcoming fluorescent fluctuation measurements were analyzed with the PCH analysis.

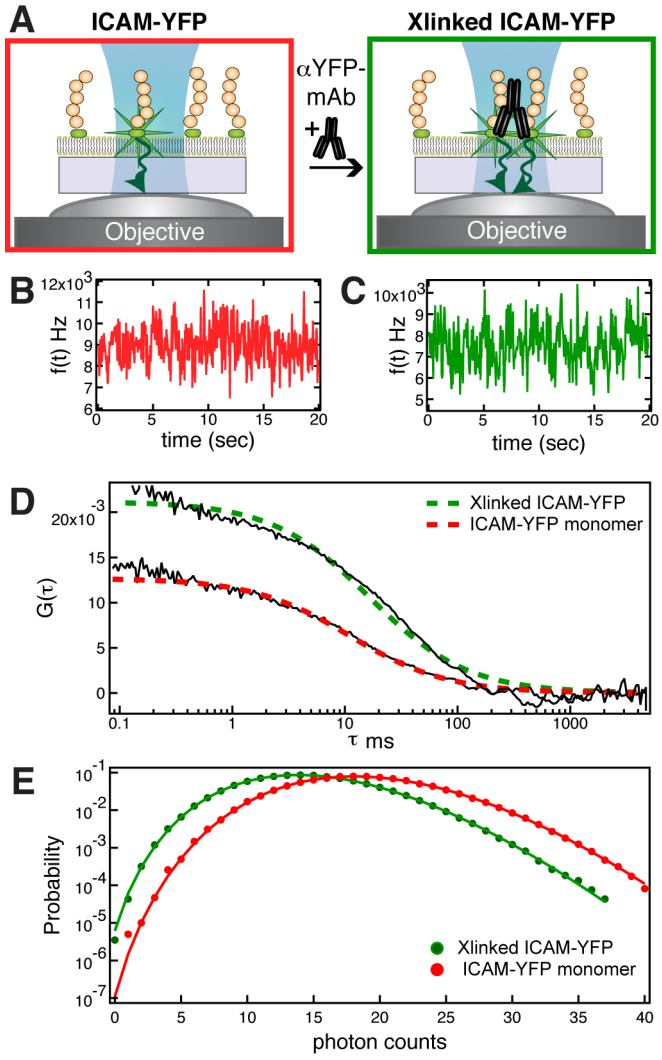

F

Parameter	ICAM-YFP Monomer	Cross-linked ICAM-YFP
B_1	1.51	1.51
N_1	77.49	40.74
B_2	—	3.01
N_2	—	11.13

Figure 3.1: Detection of ICAM-YFP dimerization on the bilayer. **(A)** Schematic of ICAM-YFP dimerization by the addition of a crosslinking antibody, αYFP mAb. Raw data measurements for ICAM-YFP monomer **(B)** and crosslinked ICAM-YFP (**C**). **(D)** Autocorrelation functions generated from raw data in **(B)** and **(C)**. The dashed lines represent the fit to equations for ICAM-YFP monomer (red) and crosslinked ICAM-YFP (green). **(E)** Photon counting histogram analyses for ICAM-YFP monomer (red) and crosslinked ICAM-YFP (green). **(F)** Table of calculated parameters for the PCH analysis. **(F)** Table of calculated parametric values for measurements taken before and after crosslinking.

3.3.2 Fluorescent fluctuation measurements reveal a gradient of LFA-1:ICAM-1 cluster sizes.

We probe the different clustered species of LFA-1:ICAM-1 complexes at the pSMAC that move in and out of the small laser excitation area. The 500 nm diameter laser spot used allows the sampling of many areas within the pSMAC with exquisite spatial precision. Upon exposure of the T cells to the SLB, we move the laser spot at 1 μm increments along the synaptic interface and take measurements (Fig. 2A). This allows us to determine how LFA-1:ICAM-1 complexes are clustered in relation to their radial position at the IS.

Interestingly, we observe bleaching, highlighted in red, of LFA-1:ICAM-1 complexes within 2 seconds of moving to a new area. Persistent fluorescent fluctuations, highlighted in blue, follow the initial photobleaching period (Fig. 2B, right). Such photobleaching events are common in fluorescent fluctuation studies, especially for ones involving cell systems [80]. It is believed that the association of fluorescent proteins with structures such as the actin cytoskeleton leads to apparent immobility within the timescale of the measurement [80]. For example, the nucleation of TCR microclusters has been found to be dependent on actin. However, TCR microclusters may grow up to the size of the laser spot and this may lead to bleaching as well.

To quantitatively analyze these bleaching events, we calculate the ratio of the bleached intensity to the total intensity. The resulting value is the fraction of ICAM-1 that exists in structures that are bleached due to their slow movement. We extend this idea and assume that the slow-moving fraction at each sampled spot is the fraction of ICAM-1 that associates with the cytoskeleton and likely exists in large LFA-1:ICAM-1 clusters, based on the proposed frictional coupling model to be discussed later. As we move the illumination spot toward the center of the cell, we observe a gradual increase in the calculated slow-moving fraction as a function of radial distance (Fig. 2B, bottom left). Figure 2B, right, shows some of the collected raw measurements taken for a single cell at the specified areas. From these graphs, the increased extent of bleaching in areas closest to the cSMAC is readily apparent. Moreover, the bleaching event is not evident in measurements on cell-free bilayers (Fig. 1B and C) or for areas on the bilayer that are adjacent to, but not interacting with, cells (Fig. 2C). Thus, the fraction of ICAM-1 in slow-moving structures, which we believe are large LFA-1:ICAM-1 complexes, increases with decreasing distance from the synaptic center.

We also analyze the persistent fluorescence fluctuations at each area with the PCH method. Data obtain from outside of the target cell was fitted to a single-species model to obtain the molecular brightness, B_1, of a single ICAM-YFP. The resulting B_1 was then used as a fixed parameter in the two-species model when analyzing the data acquired within the cell, i.e. the center (C) and areas within the pSMAC (P1, P2, P3, and P4). (Fig. 2D, left). This analysis shows an ICAM-1 population of mostly monomers, with the average size close to 1, also occupies the pSMAC (Fig. 2D, right). Our results show that two populations of LFA-1:ICAM-1 complexes exist—large clusters and ICAM-1 monomers.

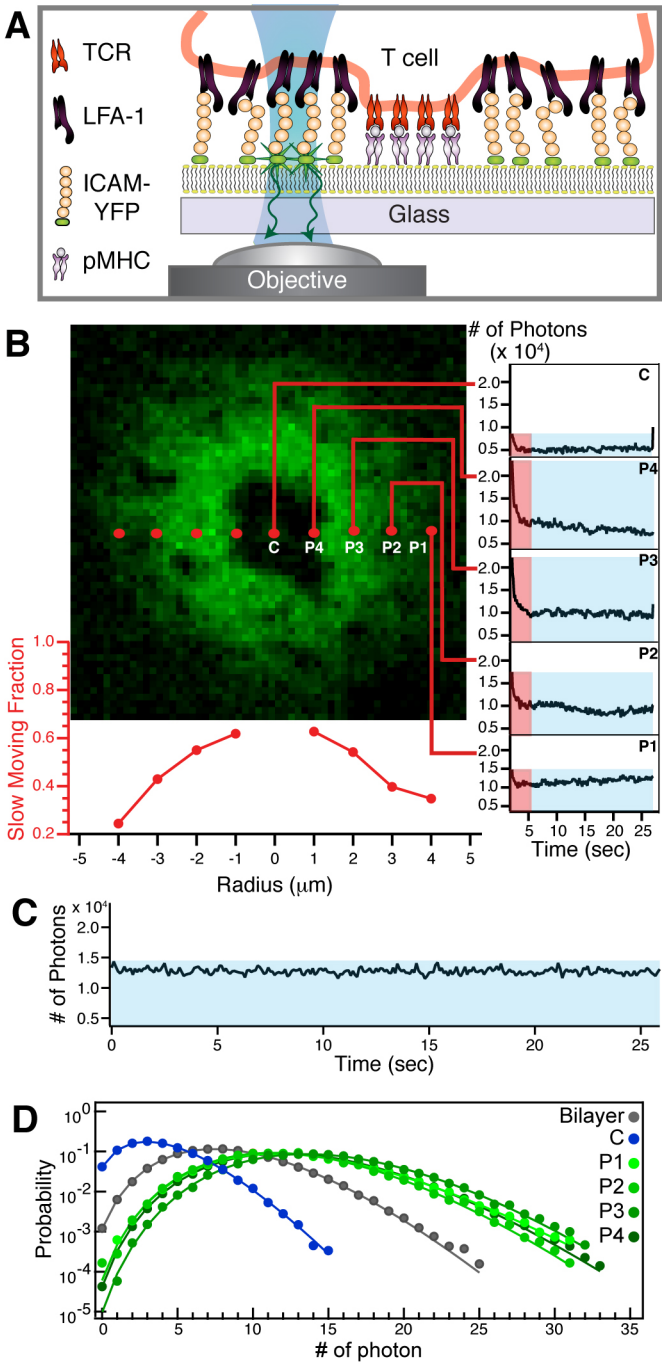

Figure 3.2: Gradient of LFA-1:ICAM-1 cluster sizes across pSMAC. **(A)** Schematic of spatially resolved illumination of areas within the synaptic interface. **(B)** Fluorescent fluctuation measurements were obtained by scanning across the synaptic interface in 1 μm increments. Red dots on the cell image indicate areas sampled. **Right** Raw data acquired at areas indicated. Region highlighted in red shows immediate bleaching after moving to a new spot and areas highlighted in blue are persistent fluctuations. **Bottom left** Graph of slow-moving fraction as a function of radial distance from the center. **(C)** Fluorescent fluctuation measurements taken at the bilayer surrounding the cell. No bleaching was observed. **(D)** PCH analysis of persistent fluctuations at various areas within the IS and surrounding bilayer.

3.3.3 LFA-1:ICAM-1 cluster size gradient persists at different ICAM-1 densities.

To test the effect of ICAM-1 concentration on LFA-1:ICAM-1 clusters, we presented ICAM-1 on the bilayer at various densities. As shown in previous work, this was readily achieved by using different concentrations of ICAM-1 in the protein solutions incubated with the bilayer for 40 minutes prior to T cell addition [33]. This appears to have no significant effect on pMHC presentation, since the cells continued to form stable synapses within the course of a typical IS experiment. Raw fluorescence fluctuation measurements display similar bleaching events as observed in Figure 3B and the slow-moving fraction at each illumination area for all cells was calculated. Figure 3A shows graphs of slow-moving fraction versus the normalized radius at corresponding ICAM-1 concentrations given in number of molecules per μm^2. The lines between the points are arbitrarily added only to distinguish each set of measurements across the pSMAC. All cells follow the same increase in the slow-moving fraction with decreasing distance from the cell center, regardless of the ICAM-1 densities.

By plotting the slow-moving fraction versus ICAM-1 concentration (Fig. 3B, blue dots), it appears that the bleaching events we observe are not a result of increased molecular crowding closer to the cSMAC. If this were the case, we would expect the slow-moving fractions at a given ICAM-1 density to collectively increase with increasing ICAM-1 densities. Instead, higher concentrations of ICAM-1 lead to decreased values for the slow-moving fractions, and this trend is most clear for ICAM-1 densities between 10 and 100 molecules per μm^2. Disparities in the ICAM-1 and LFA-1 concentrations may explain our results. Whereas we can vary the ICAM-1 density over a large range of concentrations, T cells display a finite number of LFA-1 molecules, approximately 100 molecules per μm^2. At higher ICAM-1 densities, the number of ICAM-1 molecules may exceed the number of LFA-1 available for binding [81], leading to a higher population of less clustered ICAM-1. The ICAM-1 densities of 10-100 molecules per μm^2 best fit the physiological range of ICAM-1 densities on the APC [81], and this may be why the trend in bleaching as a function of ICAM-1 density is most clear at this range.

We also use the PCH method to analyze the fluorescent fluctuations at specific areas for all cells sampled. Figure 3B (green dots) shows the plot of normalized brightness as a function of ICAM-1 density. At very high ICAM-1 densities, the brightness, normalized to the bilayer, approaches 1 for all cells. However, for ICAM-1 surface densities closer to the physiological range, the normalized brightness values are much higher, peaking at 2.5 ICAM-1 molecules per oligomer. These ICAM-1 densities appear to best reflect the native conditions of LFA-1:ICAM-1 clustering.

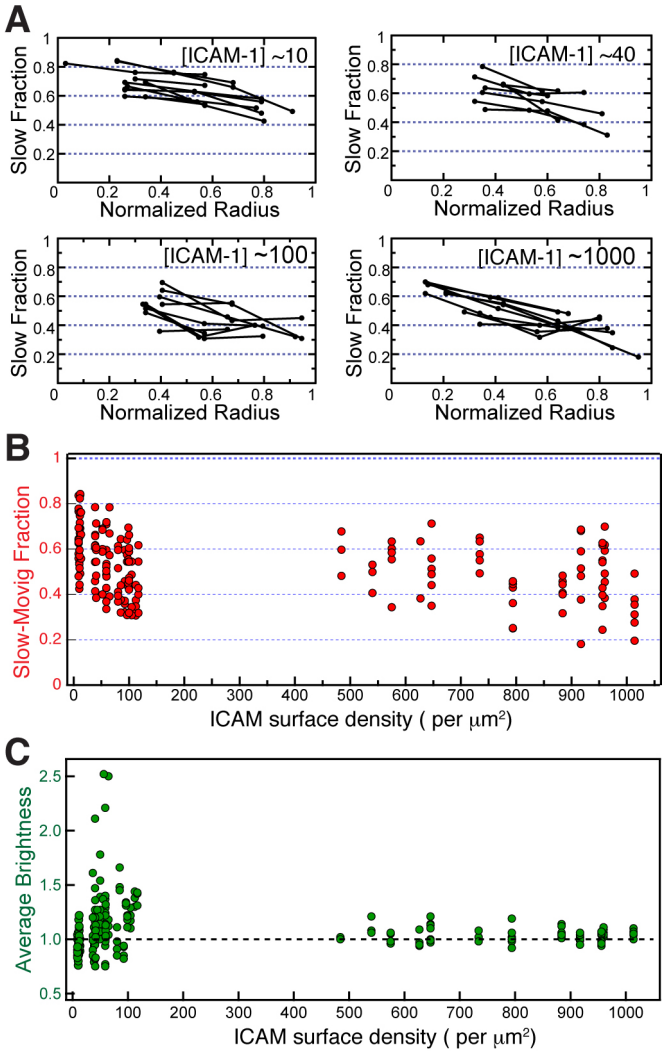

Figure 3.3: Slow-moving fractions at different densities of ICAM-YFP. **(A)** Graphs of the slow-moving fraction at specified distances from the center of the IS for the specified ICAM-YFP concentrations on the bilayer. Graphs of slow-moving fraction **(B)** and normalized brightness **(C)** as a function of ICAM-YFP surface density.

3.4 Discussion

Fluorescence fluctuations measurements and a small illumination spot allowed us to probe the intricate organization of LFA-1:ICAM-1 clusters within the IS. We detect two degrees of ICAM-1 clustering across the pSMAC—small groups of no more than 3 molecules and larger clusters that are immediately bleached upon laser illumination. The bleaching event is an indication of the fraction of ICAM-1 molecules that exists in large and/or slow-moving clusters of LFA-1:ICAM-1 complexes. In the absence of ICAM-1 interaction with LFA-1, such as in areas of the bilayer that do not interact with cells, bleaching was not observed. Therefore, the bleaching is a direct result of ICAM-1 binding to LFA-1. Furthermore, as we move toward the center, the fraction of ICAM-1 in larger clusters increases, which is determined via the extent of bleaching. It is possible that increased molecular crowding closer to the center simply leads to increased bleaching. However, the striking trend of decreasing values for slow-moving fractions with increasing ICAM-1 densities within physiologically relevant concentrations contradicts this assumption. Our data point to the existence of a gradient of

LFA-1:ICAM-1 cluster sizes across the pSMAC, in accordance with the frictional force coupling model we proposed.

As discussed in Section 2.4, the extent of protein transport by actin scales nonlinearly with the protein cluster size in the frictional force coupling model. Within the intermembrane junction of the IS, many protein cluster sizes exist (Fig. 3.4A). The total actin coupling force exerted on a specific cluster is greater than the sum of all the forces on the individual molecules that comprise the cluster. During centripetal transport, larger or denser clusters move downfield to the center of the cell, the endpoint for actin transport due to actin depolymerization. In this manner, size based sorting results (Fig. 3.4A). ICAM-YFP bleaching at the dSMAC and pSMAC, where active transport occurs, reveals that the LFA-1:ICAM-1 clusters are indeed sorted. The larger the LFA-1:ICAM-1 cluster size, the greater the coupling to actin and the extent of centripetal transport (Schematic representation, Fig. 3.4B & C). Thus, our results reveal a higher degree of organization in the IS than previously observed. Our findings contradict the proposed model that cluster stability, instead of cluster size, determines protein sorting into the different SMACs. If cluster stability were the only determining factor, then the additional degree of cluster size based protein sorting within the pSMAC would not be observed. The simplicity, consistency with our results, and ability to predict formerly unrecognized phenomena all support the frictional force coupling model as the mechanism behind IS assembly.

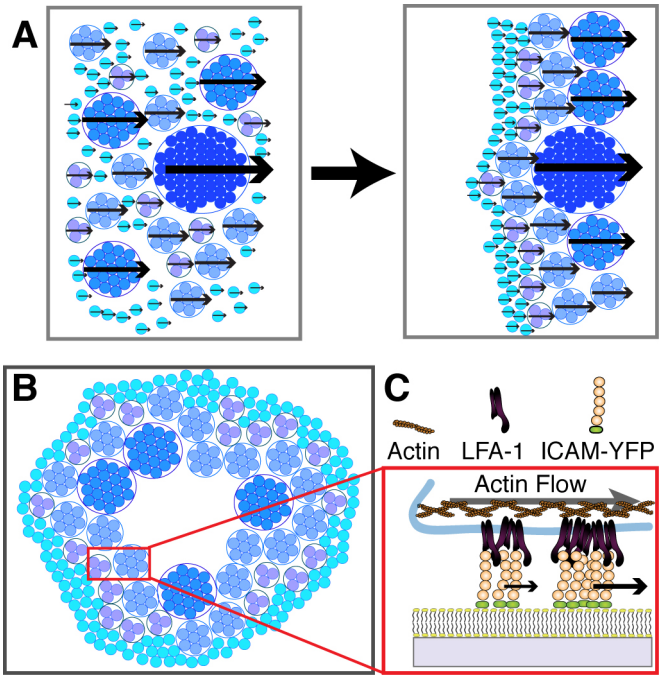

Figure 3.4: Schematic of cluster size based sorting of LFA-1:ICAM-1 complexes. **(A)** Illustration of different cluster sizes and varying actin coupling forces on each. Actin transport progresses until the driving force is balanced by competition with neighboring clusters. **(B) Top view** Schematic of cluster size-based gradient of LFA-1:ICAM-1 complexes across the pSMAC. **(C) Side view** Schematic of cluster size dependent, differential LFA-1:ICAM-1 actin transport.

3.5 Experimental Procedures

3.5.1 Cells and Reagents

Primary naïve T cells were harvested from the spleen and lymph nodes of first generation AND x B10.BR transgenic mice obtained from Jackson Laboratory (Bar Harbor, Maine). The cells were cultured and expanded to $CD4^+$ T cell blasts as described elsewhere (1, 2). The Animal Welfare and Research Committee (AWRC) approves this protocol under Animal Use Protocol #17702. Lipids were purchased from Avanti Polar Lipids (Alabaster, AL). Mouse 3E6 anti-GFP antibody, which cross-reacts with YFP, was obtained from Invitrogen (Carlsbad, CA). The MCC peptide (88-103, ANERADLIAYKQATK) was synthesized by Biosynthesis, Inc. (Lewisville TX) and other oligonucleotides were obtained from Elim Biosciences. Decahistidine-tagged ICAM-1-YFP fusion protein, its non-binding mutant and dodecahistidine-tagged MHC Class II I-E^K were expressed and purified as described [33]. The nonbinding ICAM-YFP E34D mutant was produced by site directed mutagenesis performed using the QuikChange SDM kit (Stratagene). The DNA was amplified in Top10 supercompetent cells (Invitrogen) and purified with mini- or maxi-prep kits from Qiagen. Protein expression and purification is the same as described for ICAM-YFP. Treated 40 mm coverslips were sonicated in a 50:50 mixture of isopropyl alcohol and deionized (DI) H_2O or 1% Hellmanex solution for 30 min and rinsed thoroughly. They were subsequently etched in piranha solution (4:1 H_2SO_4:H_2O_2), rinsed ten times with DI H_2O, and dried with N_2 gas right before attachment to a temperature controlled flow cell chamber (Bioptechs, Butler, PA).

3.5.2 Supported Membrane

MHC was incubated with moth cytochrome *c* (MCC) peptide for 22 hours at a final concentration of 100 mM at 37°C in pH 4.5 citrate buffer containing 0.1% bovine serum albumin (BSA). To make vesicles comprised of DOPC (98 mol%) and Ni^{2+}-NTA-DOGS (2 mol%), appropriate volumes of stock solutions were evaporated onto a 25 mL round bottom flask with a rotary evaporator (Buchi, Inc.). After drying under a stream of N_2 gas for 10 min, vesicles were hydrated. Unilamellar vesicles were formed by sonication. Standard protocol was used to deposit the SLB onto the coverslips. The SLB was incubated with 100 mM $NiCl_2$ solution to recharge the Ni^{2+}-NTA-DOGS lipids. After washing, peptide-loaded MHC and ICAM-YFP were added and incubated for 40 min in hepes/1% fetal bovine serum (FBS) buffer at room temperature. The flow cell was heated to 37°C and fluorescence fluctuation measurements were allowed to equilibrate before the addition of live murine AND CD^{4+} T cells. For the control experiments with the crosslinking antibody against YFP, mouse 3E6 full antibody (aYFP-mAb) was added at 5 mg/mL and incubated for 20 minutes.

3.5.3 Imaging

Fluorescence fluctuation spectroscopy measurements were performed on a home-built FCS apparatus integrated into a Nikon TE2000 inverted fluorescence microscope based on a previous design [44]. In brief, a 4 μW 488nm laser beam (Stabilite 2018-RM, Newport Corp.) was coupled into the light path of the microscope by a dichroic mirror and focused by a 100X TIRF objective (Nikon Corp., Tokyo, Japan) onto the sample to excite the fluorescent probes. The emission light was filtered by a 488 nm notch filter (Kaiser Optical Systems, Ann Arbor, MI) and a confocal pinhole (50 μm diameter, Thorlabs, Newton, NJ), then focused into an avalanche photo diode (APD) (Perkin&Elmer, Canada). The photon arrival times were recorded by a counter card (Flex01LQ-05, correlator.com) and the auto-correlation function of the signal was calculated by a hardware correlator (correlator.com, Bridgewater, NJ) in real time. The histogram of recorded photon counts were later analyzed using the Globals software package developed at the Laboratory for Fluorescence Dynamics at the University of Illinois at Urbana-Champaign. The excitation volume was calibrated at room temperature (25°C) before each experiment using a dye solution of fluorescein

(Sigma, MO) (50 nM in 25 mM Tris buffer, pH 10). The diffusion coefficient of the dye was set to 300 $\mu m^2/s$ (ref) to determine the waist of the laser beam. The temperature controlled flow cell chambers were mounted on a motorized stage (MS-2000 XYZ , Applied Scientific Instrument, Eugene, OR) for precise position control. Epifluorescence images were taken before and after FCS measurements with the MetaMorph software package (Molecular Devices) and a Cascade 512B EMCCD camera (Roper).

3.5.4 Measurements

Prior to the addition of T cells, fluorescence fluctuations of ICAM-YFP were recorded at several different positions to ensure the 2-D fluidity and uniformity of the supported membrane. Only samples without detectable photobleaching were used for the T cell experiments. For each T cell observed, the fluorescence fluctuation measurements were performed along the diameter of the IS. The data acquisition started from outside of the cell and the sample was moved along the diameter in 1 μm increments every 25 s. All the measurements were performed between 5 min to 65 min after exposure of T cells to the SLB.

3.5.5 Data Analysis

The autocorrelation functions, $G(\tau)$, were fitted to analytical expressions of normal 2-D diffusion using a nonlinear Levenberg-Marquardt algorithm to recover the G(0) values. For single species samples, the average number of molecules N within the excitation area is

$$G(0) = \frac{1}{N_1}$$

For two species samples, G(0) is the sum of each species's G(0) value weighted by the square of the fractional intensity, B_1 and B_2 [76].

$$G(0) = \frac{B_1^2 N_1 + B_2^2 N_2}{(B_1 N_1 + B_2 N_2)^2}$$

For PCH analysis, the recorded photon arrivals were first binned in 1 ms sampling time to obtain photon counts. The histogram of the photon counts was then normalized to yield photon probability distribution. In antibody-crosslinking experiments of ICAM-YFP, membrane measurements were first taken before the addition of the antibody. The data were fitted to a theoretical distribution function of single species to extract the molecular brightness B_1 of a single ICAM-YFP and the average number of ICAM-YFP molecules. The resulting B_1 was then used as a fixed fitting parameter in a two-species model to analyze the data taken after antibody crosslinking of ICAM-YFP. In the two-species PCH analysis, the distribution of photon counts is described with two parameters for each species: the molecular brightness and the average number of particles in the excitation area. Similarly, in the T cell experiments, data acquired from the outside of each target cell was used to obtain local molecular brightness B_1 and local surface density of ICAM-YFP. Data acquired inside of the cell was then fitted to a two-species model with the fixed single ICAM-YFP brightness B_1. The resulting four parameters, namely brightness of single ICAM-YFP (B_1), number of single ICAM-YFP (N_1), average brightness of clustered ICAM-YFP (B_c), and average number of ICAM-YFP clusters (N_c) were then used to calculate the normalized average brightness of ICAM-YFP clusters, B_{AV}.

$$B_{AV} = \frac{1}{B_1} \frac{B_1 N_1 + B_C N_C}{N_1 + N_C}$$

Chapter 4

Concluding Remarks

In this dissertation, we have demonstrated that cluster size can regulate protein sorting at various levels in the IS. The results presented here support the frictional force coupling model we propose and provide insight into the IS mechanism of formation. However, forthcoming additional experiments are necessary to rigorously support our claims. First, we will confirm that LFA-1 binding to ICAM-1—and not molecular crowding in the closely apposed intermembrane space—is the cause of the observed bleaching events. In this experiment, we will present both an ICAM-YFP mutant that does not bind to LFA-1 and non-fluorescent, LFA-1 binding ICAM-1 (dark ICAM-1) with activating pMHC on the fluid bilayer. This preserves the intermembrane junction through dark ICAM-1:LFA-1 binding but eliminates clustering and actin coupling of the fluorescently observed ICAM-YFP due to impaired LFA-1 binding. We predict that ICAM-YFP behavior under the cell will be similar to that of ICAM-YFP away from cells. More importantly, no bleaching event should be detected.

The use of pharmacological inhibitors targeting the actin cytoskeleton will also give insight into whether the slow-moving structures are interacting with actin. Myosin II may also be targeted since current research suggests that it helps mediate centripetal actin transport of proteins in the IS. Blebbistatin is a widely used drug against Myosin II. The addition of Latrunculin A and cytochalasin should disrupt actin polymerization, abolishing IS formation and cluster size-based sorting. These inhibitors may be added to the cells prior to bilayer exposure. Alternatively, the addition of these drugs to cells that already display the IS pattern should lead to the observed loss of the pre-existing cluster size gradient across the pSMAC. In addition to cytoskeletal drugging experiments, LFA-1 coupling to actin may be investigated by modifying the adaptor protein talin. Talin has two domains: an actin binding tail and a LFA-1 binding head. Overexpression of the talin head alone can lead to decoupling of LFA-1 from the actin dynamics. It would be interesting to see if LFA-1:ICAM-1 clustering occurs independent of actin, since it has been found that TCR microcluster nucleation is actin dependent. We expect that LFA-1:ICAM-1 clusters would not become sorted at the IS due to loss of actin transport.

Ultimately, we wish to resolve the number of molecules within the LFA-1:ICAM-1 clusters. This can be achieved in two ways. First, we can use pulse interleaved excitation to collect fluorescence fluctuation measurements on much faster time scales, before any bleaching can occur. This method is useful not only in determining the number of molecules in each cluster but also in determining whether any FRET or quenching occurs due to homo-dimerization. Second, we can make an ICAM-1-mEOS2 mutant and detect the gradient in cluster sizes across the pSMAC with Photoactivation Localization Microscopy (PALM) [82]. PALM allows the resolution of particles well below the diffraction limit by sequential activation of photoswitchable fluorophores. To do this, samples must be fixed and data collection may take hours. The static nature of PALM makes it a good complementary method to use in conjunction with the more dynamic, live cell observations that fluorescent fluctuation measurements allow.

The set of experiments we propose here focuses mainly on the mechanics of LFA-1:ICAM-1 transport and sorting by actin. LFA-1:ICAM-1 complexes are ideal for the study of transport processes due to the ease with which their spatial distribution may be altered and studied, as we have demonstrated in Chapter 2. However, we believe that our findings may be extended to other proteins in the IS and help elucidate the universal mechanism of spatial localization in the IS. Moreover, the well-orchestrated events of protein spatial patterning and the high degree of organization we discovered suggest that protein sorting at various length scales modulates cell activation. We hypothesize that the spatial organization at the IS regulates downstream signaling as well as signal attenuation. The functional relevance of the LFA-1:ICAM-1 ring to TCR signaling is a special area of interest that we are poised to explore. To probe differential protein sorting without introducing non-specific perturbations, we have already developed s set of lithographic and protein tethering techniques combined with supported lipid bilayers to induce spatial reconfiguration of protein patterns in the IS. In current and future research work, we plan to investigate how molecular- and micron-scale clusters lead to protein targeting and subsequent signal transduction—a motif that is relevant to many biological signaling systems beyond the IS.

Chapter 5

References

[1] Richard Goldsby, *Kuby immunology*, 4th ed. (New York: W.H. Freeman, 2000).

[2] JC Cerottini, "Cell-mediated cytotoxicity, allograft rejection, and tumor immunity.," *Adv Immunol* 18 (1974): 67-132.

[3] Jerrold Schwaber and Edward P. Cohen, "Human × Mouse Somatic Cell Hybrid Clone secreting Immunoglobulins of both Parental Types," *Nature* 244, no. 5416 (8, 1973): 444-447.

[4] JP Allison, BW McIntyre, and D Bloch, "Tumor-specific antigen of murine T-lymphoma defined with monoclonal antibody," *J Immunol* 129, no. 5 (November 1, 1982): 2293-2300.

[5] S. C. Meuer, "Clonotypic structures involved in antigen-specific human T cell function. Relationship to the T3 molecular complex," *Journal of Experimental Medicine* 157, no. 2 (2, 1983): 705-719.

[6] T A Springer et al., "The lymphocyte function-associated LFA-1, CD2, and LFA-3 molecules: cell adhesion receptors of the immune system," *Annual Review of Immunology* 5 (1987): 223-252.

[7] B E Bierer et al., "The Biologic Roles of CD2, CD4, and CD8 in T-Cell Activation," *Annual Review of Immunology* 7, no. 1 (4, 1989): 579-599.

[8] P. Anton van der Merwe et al., "Topology of the CD2-CD48 cell-adhesion molecule complex: implications for antigen recognition by T cells," *Current Biology* 5, no. 1 (January 1995): 74-84.

[9] Barry A. Fields et al., "Crystal structure of a T-cell receptor [beta]-chain complexed with a superantigen," *Nature* 384, no. 6605 (November 14, 1996): 188-192.

[10] E L Reinherz et al., "The crystal structure of a T cell receptor in complex with peptide and MHC class II," *Science (New York, N.Y.)* 286, no. 5446 (December 3, 1999): 1913-1921.

[11] RL Brady et al., "Crystal structure of domains 3 and 4 of rat CD4: relation to the NH2-terminal domains," *Science* 260, no. 5110 (May 14, 1993): 979-983.

[12] George F. Gao et al., "Crystal structure of the complex between human CD8[alpha][alpha] and HLA-A2," *Nature* 387, no. 6633 (June 5, 1997): 630-634.

[13] C. R. F. Monks et al., "Three-dimensional segregation of supramolecular activation clusters in T cells," *Nature* 395, no. 6697 (1998): 82-86.

[14] Kenneth G. Johnson et al., "A supramolecular basis for CD45 tyrosine phosphatase regulation in sustained T cell activation," *Proceedings of the National Academy of Sciences of the United States of America* 97, no. 18 (August 29, 2000): 10138-10143.

[15] S. Y. Qi, J. T. Groves, and A. K. Chakraborty, "Synaptic pattern formation during cellular recognition," *Proceedings of the National Academy of Sciences of the United States of America* 98, no. 12 (2001): 6548-6553.

[16] F. D. Batista, D. Iber, and M. S. Neuberger, "B cells acquire antigen from target cells after synapse formation," *Nature* 411, no. 6836 (2001): 489-494.

[17] M. S. Fassett et al., "Signaling at the inhibitory natural killer cell immune synapse regulates lipid raft polarization but not class I MHC clustering," *Proceedings of the National Academy of Sciences of the United States of America* 98, no. 25 (2001): 14547-14552.

[18] Jean-Nicolas Tournier and Anne Quesnel Hellmann, "Neuro-immune connections: evidence for a neuro-immunological synapse," *Trends in Immunology* 24, no. 3 (March 2003): 114-115.

[19] Eric Hailman et al., "Immature CD4(+)CD8(+) thymocytes form a multifocal immunological synapse with sustained tyrosine phosphorylation," *Immunity* 16, no. 6 (June 2002): 839-848.

[20] A. Grakoui et al., "The immunological synapse: A molecular machine controlling T cell activation," *Science* 285, no. 5425 (1999): 221-227.

[21] C. Wulfing, M. D. Sjaastad, and M. M. Davis, "Visualizing the dynamics of T cell activation: Intracellular adhesion molecule 1 migrates rapidly to the T cell/B cell interface and acts to sustain calcium levels," *Proceedings of the National Academy of Sciences of the United States of America* 95, no. 11 (1998): 6302-6307.

[22] S C Kinsky and R A Nicolotti, "Immunological Properties of Model Membranes," *Annual Review of Biochemistry* 46, no. 1 (7, 1977): 49-67.

[23] G M Humphires and H M McConnell, "Antigen mobility in membranes and complement-medical immune attack," *Proceedings of the National Academy of Sciences of the United States of America* 72, no. 7 (July 1975): 2483-2487.

[24] A A Brian and H M McConnell, "Allogeneic stimulation of cytotoxic T cells by supported planar membranes," *Proceedings of the National Academy of Sciences of the United States of America* 81, no. 19 (October 1984): 6159-6163.

[25] Larry T. Mimms et al., "Phospholipid vesicle formation and transmembrane protein incorporation using octyl glucoside," *Biochemistry* 20, no. 4 (February 1, 1981): 833-840.

[26] S H Herrmann and M F Mescher, "Secondary cytolytic T lymphocyte stimulation by purified H-2Kk in liposomes," *Proceedings of the National Academy of Sciences of the United States of America* 78, no. 4 (April 1981): 2488-2492.

[27] Leonid B. Marcolis, "Cell interaction with model membranes probing, modification and simulation of cell surface functions," *Biochimica et Biophysica Acta (BBA) - Reviews on Biomembranes* 779, no. 2 (June 25, 1984): 161-189.

[28] T A Springer, "Adhesion receptors of the immune system," *Nature* 346, no. 6283 (August 2, 1990): 425-434.

[29] M L Dustin et al., "Anchoring mechanisms for LFA-3 cell adhesion glycoprotein at membrane surface," *Nature* 329, no. 6142 (November 29, 1987): 846-848.

[30] Y. Kaizuka et al., "Mechanisms for segregating T cell receptor and adhesion molecules during immunological synapse formation in Jurkat T cells," *Proc Natl Acad Sci U S A* 104, no. 51 (2007): 20296-301.

[31] Jwa-Min Nam et al., "A Fluid Membrane-Based Soluble Ligand-Display System for Live-Cell Assays," *ChemBioChem* 7, no. 3 (2006): 436-440.

[32] E W Kubalek, S F Le Grice, and P O Brown, "Two-dimensional crystallization of histidine-tagged, HIV-1 reverse transcriptase promoted by a novel nickel-chelating lipid," *Journal of Structural Biology* 113, no. 2 (October 1994): 117-123.

[33] J. A. Nye and J. T. Groves, "Kinetic control of histidine-tagged protein surface density on supported lipid bilayers," *Langmuir* 24, no. 8 (2008): 4145-4149.

[34] Gudrun Stengel, Raphael Zahn, and Fredrik Höök, "DNA-Induced Programmable Fusion of Phospholipid Vesicles," *Journal of the American Chemical Society* 129, no. 31 (2007): 9584-9585.

[35] Chiaki Yoshina-Ishii et al., "General Method for Modification of Liposomes for Encoded Assembly on Supported Bilayers," *Journal of the American Chemical Society* 127, no. 5 (February 1, 2005): 1356-1357.

[36] K. D. Mossman et al., "Altered TCR signaling from geometrically repatterned immunological synapses," *Science* 310, no. 5751 (2005): 1191-1193.

[37] B. Manz, C.-H. Yu, and J. Groves, *in preparation*

[38] Michaela Schwarzenbacher et al., "Micropatterning for quantitative analysis of protein-protein interactions in living cells," *Nat Meth* 5, no. 12 (December 2008): 1053-1060.

[39] Keyue Shen et al., "Self-Aligned Supported Lipid Bilayers for Patterning the Cell–Substrate Interface," *Journal of the American Chemical Society* 131, no. 37 (2009): 13204-13205.

[40] "Immunity - The Balance between T Cell Receptor Signaling and Degradation at the Center of the Immunological Synapse Is Determined by Antigen Quality," http://www.cell.com/immunity/abstract/S1074-7613(08)00366-X.

[41] S Cemerski et al., "The Balance between T Cell Receptor Signaling and Degradation at the Center of the Immunological Synapse Is Determined by Antigen Quality," *Immunity* 29, no. 3 (9, 2008): 414-422.

[42] Saso Cemerski et al., "The Stimulatory Potency of T Cell Antigens Is Influenced by the Formation of the Immunological Synapse," *Immunity* 26, no. 3 (March 23, 2007): 345-355.

[43] B. Manz, R. Petit, B. L. Jackson, J. T. Groves, *in review*

[44] Bjorn F Lillemeier et al., "TCR and Lat are expressed on separate protein islands on T cell membranes and concatenate during activation," *Nat Immunol* 11, no. 1 (January 2010): 90-96.

[45] Tadashi Yokosuka et al., "Newly generated T cell receptor microclusters initiate and sustain T cell activation by recruitment of Zap70 and SLP-76," *Nat Immunol* 6, no. 12 (December 2005): 1253-1262.

[46] Stephen C Bunnell et al., "Persistence of cooperatively stabilized signaling clusters drives T-cell activation," *Molecular and Cellular Biology* 26, no. 19 (October 2006): 7155-7166.

[47] Adam D. Douglass and Ronald D. Vale, "Single-Molecule Microscopy Reveals Plasma Membrane Microdomains Created by Protein-Protein Networks that Exclude or Trap Signaling Molecules in T Cells," *Cell* 121, no. 6 (June 17, 2005): 937-950.

[48] Bunnell et al., "Persistence of cooperatively stabilized signaling clusters drives T-cell activation."

[49] Junsang Doh and Darrell J. Irvine, "Immunological synapse arrays: Patterned protein surfaces that modulate immunological synapse structure formation in T cells" 103, no. 15 (April 11, 2006): 5700-5705.

[50] Rajat Varma et al., "T Cell Receptor-Proximal Signals Are Sustained in Peripheral Microclusters and Terminated in the Central Supramolecular Activation Cluster," *Immunity* 25, no. 1 (July 2006): 117-127.

[51] A. L. DeMond et al., "T cell receptor microcluster transport through molecular mazes reveals mechanism of translocation," *Biophys J* 94, no. 8 (2008): 3286-92.

[52] B. Graf, T. Bushnell, and J. Miller, "LFA-1-Mediated T cell costimulation through increased localization of TCR/Class II complexes to the central supramolecular activation cluster and exclusion of CD45 from the immunological synapse," *Journal of Immunology* 179, no. 3 (2007): 1616-1624.

[53] D. D. Billadeau, J. C. Nolz, and T. S. Gomez, "Regulation of T-cell activation by the cytoskeleton," *Nature Reviews Immunology* 7, no. 2 (2007): 131-143.

[54] R. Evans et al., "Integrins in immunity," *Journal of Cell Science* 122, no. 2 (2009): 215-225.

[55] T. Ilani et al., "Immune synapse formation requires ZAP-70 recruitment by ezrin and CD43 removal by moesin," *Journal of Cell Biology* 179, no. 4 (2007): 733-746.

[56] G. Campi, R. Varma, and M. L. Dustin, "Actin and agonist MHC-peptide complex-dependent T cell receptor microclusters as scaffolds for signaling," *Journal of Experimental Medicine* 202, no. 8 (2005): 1031-1036.

[57] M. Kim, C. V. Carman, and T. A. Springer, "Bidirectional transmembrane signaling by cytoplasmic domain separation in integrins," *Science* 301, no. 5640 (2003): 1720-5.

[58] M. L. Dustin et al., "Identification of self through two-dimensional chemistry and synapses," *Annual Review of Cell and Developmental Biology* 17 (2001): 133-157.

[59] S. Pont et al., "Identification of 5-Topographic Domains of the Mouse Lfa-1 Molecule - Subunit Assignment and Functional Involvement in Lymphoid-Cell Interactions," *Journal of Immunology* 136, no. 10 (1986): 3750-3759.

[60] A. L. DeMond and J. T. Groves, "Interrogating the T cell synapse with patterned surfaces and photoactivated proteins," *Curr Opin Immunol* 19, no. 6 (2007): 722-7.

[61] J. T. Groves, N. Ulman, and S. G. Boxer, "Micropatterning fluid lipid bilayers on solid supports," *Science* 275, no. 5300 (1997): 651-653.

[62] J. T. Groves et al., "Substrate-membrane interactions: Mechanisms for imposing patterns on a fluid bilayer membrane," *Langmuir* 14, no. 12 (1998): 3347-3350.

[63] Groves, Ulman, and Boxer, "Micropatterning fluid lipid bilayers on solid supports."

[64] W. J. Galush, J. A. Nye, and J. T. Groves, "Quantitative fluorescence microscopy using supported lipid bilayer standards," *Biophysical Journal* 95, no. 5 (2008): 2512-2519.

[65] J. T. Groves, S. G. Boxer, and H. M. McConnell, "Electric field-induced reorganization of two-component supported bilayer membranes," *Proc Natl Acad Sci U S A* 94, no. 25 (1997): 13390-5.

[66] J. T. Groves, S. G. Boxer, and H. M. McConnell, "Electric field-induced critical demixing in lipid bilayer membranes," *Proc Natl Acad Sci U S A* 95, no. 3 (1998): 935-8.

[67] T. Yokosuka et al., "Spatiotemporal Regulation of T Cell Costimulation by TCR-CD28 Microclusters and Protein Kinase C theta Translocation," *Immunity* 29, no. 4 (2008): 589-601.

[68] K. Choudhuri et al., "T-cell receptor triggering is critically dependent on the dimensions of its peptide-MHC ligand," *Nature* 436, no. 7050 (2005): 578-582.

[69] T. R. Weikl, J. T. Groves, and R. Lipowsky, "Pattern formation during adhesion of multicomponent membranes," *Europhysics Letters* 59, no. 6 (2002): 916-922.

[70] R. Parthasarathy and J. T. Groves, "Protein patterns at lipid bilayer junctions," *Proceedings of the National Academy of Sciences of the United States of America* 101, no. 35 (2004): 12798-12803.

[71] Jay T. Groves, "Molecular Organization and Signal Transduction at Intermembrane Junctions," *Angewandte Chemie International Edition* 44, no. 23 (2005): 3524-3538.

[72] Boryana N. Manz and Jay T. Groves, "Spatial organization and signal transduction at intercellular junctions," *Nat Rev Mol Cell Biol* advance online publication (March 31, 2010), http://dx.doi.org/10.1038/nrm2883.

[73] S. K. Bromley et al., "The immunological synapse," *Annu Rev Immunol* 19 (2001): 375-96.

[74] Niña C. Hartman, Jeffrey A. Nye, and Jay T. Groves, "Cluster size regulates protein sorting in the immunological synapse," *Proceedings of the National Academy of Sciences* 106, no. 31 (2009): 12729-12734.

[75] Y. Kaizuka et al., "The coreceptor CD2 uses plasma membrane microdomains to transduce signals in T cells," *The Journal of Cell Biology* 185, no. 3 (4, 2009): 521-534.

[76] Thompson, N. L. Fluorescence Correlation Spectroscopy. In *Topics in Fluorescence Spectroscopy*; Lakowicz, J. R., II, Ed.; Plenum Press: New York, 1995; pp 337−410.

[77] Yan Chen, Li-Na Wei, and Joachim D. Müller, "Probing protein oligomerization in living cells with fluorescence fluctuation spectroscopy," *Proceedings of the National Academy of Sciences of the United States of America* 100, no. 26 (December 23, 2003): 15492-15497.

[78] Y Chen et al., "The photon counting histogram in fluorescence fluctuation spectroscopy," *Biophysical Journal* 77, no. 1 (July 1999): 553-567.

[79] Yan Chen et al., "Molecular brightness characterization of EGFP in vivo by fluorescence fluctuation spectroscopy." *Biophysical Journal* 82, no. 1 Pt 1 (January 2002): 133-144.

[80] J Skinner, "Fluorescence Fluctuation Spectroscopy in the Presence of Immobile Fluorophores⋆," *Biophysical Journal* 94, no. 6 (3, 2008): 2349-2360.

[81] Springer et al., "The lymphocyte function-associated LFA-1, CD2, and LFA-3 molecules."

[82] S Hess, T Girirajan, and M Mason, "Ultra-High Resolution Imaging by Fluorescence Photoactivation Localization Microscopy," *Biophysical Journal* 91, no. 11 (12, 2006): 4258-4272.